Soluble α-klotho and heparin modulate the pathologic cardiac actions of fibroblast growth factor 23 in chronic kidney disease

OPEN

Christopher Yanucil[1], Dominik Kentrup[1,2], Isaac Campos[1], Brian Czaya[1], Kylie Heitman[1], David Westbrook[1], Gunars Osis[1], Alexander Grabner[3], Adam R. Wende[4], Julian Vallejo[5], Michael J. Wacker[5], Jose Alberto Navarro-Garcia[6], Gema Ruiz-Hurtado[6], Fuming Zhang[7], Yuefan Song[8], Robert J. Linhardt[7,8], Kenneth White[9], Michael S. Kapiloff[10,11] and Christian Faul[1]

[1]*Division of Nephrology, Department of Medicine, The University of Alabama at Birmingham, Birmingham, Alabama, USA;* [2]*Division of Nephrology and Hypertension, Center for Translational Metabolism and Health, Feinberg Cardiovascular and Renal Research Institute, Northwestern University, Chicago, Illinois, USA;* [3]*Division of Nephrology, Department of Medicine, Duke University School of Medicine, Durham, North Carolina, USA;* [4]*Division of Molecular & Cellular Pathology, Department of Pathology, The University of Alabama at Birmingham, Birmingham, Alabama, USA;* [5]*Department of Molecular Biosciences, University of Missouri-Kansas City School of Medicine, Kansas City, Missouri, USA;* [6]*Cardiorenal Translational Laboratory, Institute of Research, Hospital Universitario 12 de Octubre, Madrid, Spain;* [7]*Department of Chemical and Biological Engineering, Center for Biotechnology and Interdisciplinary Studies, Rensselaer Polytechnic Institute, Troy, New York, USA;* [8]*Department of Chemistry and Chemical Biology, Center for Biotechnology and Interdisciplinary Studies, Rensselaer Polytechnic Institute, Troy, New York, USA;* [9]*Department of Medical and Molecular Genetics, Indiana University School of Medicine, Indianapolis, Indiana, USA;* [10]*Department of Ophthalmology, Stanford Cardiovascular Institute, Stanford University, Palo Alto, California, USA; and* [11]*Department of Medicine, Stanford Cardiovascular Institute, Stanford University, Palo Alto, California, USA*

Fibroblast growth factor (FGF) 23 is a phosphate-regulating hormone that is elevated in patients with chronic kidney disease and associated with cardiovascular mortality. Experimental studies showed that elevated FGF23 levels induce cardiac hypertrophy by targeting cardiac myocytes via FGF receptor isoform 4 (FGFR4). A recent structural analysis revealed that the complex of FGF23 and FGFR1, the physiologic FGF23 receptor in the kidney, includes soluble α-klotho (klotho) and heparin, which both act as co-factors for FGF23/FGFR1 signaling. Here, we investigated whether soluble klotho, a circulating protein with cardio-protective properties, and heparin, a factor that is routinely infused into patients with kidney failure during the hemodialysis procedure, regulate FGF23/FGFR4 signaling and effects in cardiac myocytes. We developed a plate-based binding assay to quantify affinities of specific FGF23/FGFR interactions and found that soluble klotho and heparin mediate FGF23 binding to distinct FGFR isoforms. Heparin specifically mediated FGF23 binding to FGFR4 and increased FGF23 stimulatory effects on hypertrophic growth and contractility in isolated cardiac myocytes. When repetitively injected into two different mouse models with elevated serum FGF23 levels, heparin aggravated cardiac hypertrophy. We also developed a novel procedure for the synthesis and purification of recombinant soluble klotho, which showed anti-hypertrophic effects in FGF23-treated cardiac myocytes. Thus, soluble klotho and heparin act as independent FGF23 co-receptors with opposite effects on the pathologic actions of FGF23, with soluble klotho reducing and heparin increasing FGF23-induced cardiac hypertrophy. Hence, whether heparin injections during hemodialysis in patients with extremely high serum FGF23 levels contribute to their high rates of cardiovascular events and mortality remains to be studied.

Kidney International (2022) ■, ■–■; https://doi.org/10.1016/j.kint.2022.03.028

KEYWORDS: cardiac hypertrophy; chronic kidney disease; fibroblast growth factor 23; heparin; klotho; phosphate metabolism

Translational Statement

Patients on hemodialysis have extremely high fibroblast growth factor 23 (FGF23) levels, and during dialysis, they receive infusions of heparin as a blood thinner. Our experimental studies show that heparin acts as a cofactor that increases FGF23's binding affinity for the cardiac FGF23 receptor and thereby aggravates the pathologic actions of FGF23 on the heart. Hemodialysis does not reduce the cardiovascular risk of patients with end-stage renal disease, and future clinical studies should test whether frequent heparin infusions contribute to the extremely high mortality rates in these patients and whether removal of heparin from the dialysis process might improve cardiac outcomes and survival.

Correspondence: *Christian Faul, Division of Nephrology, Department of Medicine, The University of Alabama at Birmingham, Tinsley Harrison Tower 611L, 1720 2nd Avenue South, Birmingham, Alabama 35294, USA. E-mail: cfaul@uabmc.edu*

Received 31 March 2021; revised 14 March 2022; accepted 29 March 2022

Fibroblast growth factor (FGF) 23 is a hormone that serves as a major regulator of phosphate metabolism.[1] In response to elevations in serum phosphate levels, such as after food intake, FGF23 is secreted by the bone and targets the kidney via FGF receptor (FGFR) isoform 1c

(FGFR1c) and the coreceptor α-klotho (called "klotho" from here on), resulting in the induction of Ras/mitogen-activated protein kinase (MAPK) signaling.[2–4] By doing so, FGF23 reduces surface expression of sodium-phosphate cotransporters in kidney proximal tubular cells and thereby kidney phosphate uptake, resulting in increased urinary phosphate excretion and a reduction in systemic phosphate levels.[5–7] Because the kidney is the only organ to excrete phosphate, reduced kidney function results in elevations of serum phosphate. Beginning in early stages of chronic kidney disease (CKD), FGF23 levels rise progressively in an attempt to maintain normal phosphate levels.[8] In patients with end-stage renal disease, who require dialysis for survival, serum FGF23 concentrations reach 1000-fold above normal values but fail to promote kidney phosphate excretion as kidney function and FGF23 responsiveness decline.[9–11]

Over the past decade, translational research from our group and others has indicated that FGF23 can affect different cell types outside the kidney and thereby contribute to various pathologic alterations associated with CKD.[12] We found that elevated FGF23 levels can directly target cardiac myocytes[13,14] and hepatocytes,[15] which do not express klotho, thereby implying that the presence of klotho is not a prerequisite for the FGF23 responsiveness of cells. We have shown in cell culture and in animal studies that in the absence of klotho, high levels of FGF23 can directly target cardiac myocytes specifically via FGFR isoform 4 (FGFR4) and activate the phospholipase Cγ (PLCγ)/calcineurin/nuclear factor of activated T cell (NFAT) signaling cascade, thereby inducing cardiac hypertrophy.[16,17] Our studies suggest that pharmacologic FGFR4 blockade might serve as a novel therapeutic option to prevent or treat pathologic cardiac remodeling in CKD (also called *uremic cardiomyopathy*).

Such novel mechanistic findings might be of high clinical relevance, as CKD is a public health epidemic that affects ∼26 million Americans and many more individuals worldwide.[18] The presence of CKD increases the risk of premature death, and cardiovascular disease is the leading cause at all stages of CKD.[19,20] Cardiac hypertrophy is an important mechanism of cardiovascular injury in CKD that contributes to diastolic dysfunction, heart failure, arrhythmia, and sudden death.[21] Cardiac hypertrophy affects 50% to 70% of patients during intermediate stages of CKD and up to 90% by the time they reach dialysis.[22–24] The molecular pathways responsible for cardiac hypertrophy in CKD remain uncertain, and existing treatments improve outcomes only modestly.[25–28] For example, hypertension is common in CKD, and it has been hypothesized that cardiac hypertrophy develops as a result of pressure overload.[29] However, the correction of hypertension in animal models with kidney injury does not prevent hypertrophy.[30–32] More recent studies suggest that circulating prohypertrophic factors may initiate specific signal transduction events in the myocardium, thereby affecting cardiac structure and function independent of mechanical stress,[33,34] with FGF23 being one of them.

FGF23 is a member of the FGF family that comprises 18 secreted proteins that have diverse functions in development and metabolism.[35] The biological effects of all FGFs are mediated by binding to 1 of the 4 FGFR isoforms (FGFR1–4) that belong to the superfamily of receptor tyrosine kinases.[36] Alternative splicing in the juxtamembrane region of FGFR1 to 3 produces b and c variants with different biological impacts on the basis of their distinct ligand-binding spectrum. Paracrine FGFs, such as FGF1 and FGF2, bind heparan sulfate (HS), which functions as an FGFR coreceptor.[36] HS promotes the formation of a stable FGF/FGFR/HS ternary complex as well as FGFR dimerization, leading to the formation of a symmetric signaling complex.[37,38] Compared with paracrine FGFs, the subfamily of endocrine FGFs, that is, FGF19, FGF21, and FGF23, have intrinsically low binding affinity for HS.[39–42] Instead of HS, endocrine FGFs use a family of single-pass transmembrane proteins, known as klotho for FGF23 and β-klotho for FGF19 and FGF21, to promote efficient FGFR binding on specific cell types.[41]

Klotho is a single-pass transmembrane protein that is mainly expressed in the kidney where, in combination with FGFR1c, it mediates the stimulating effects of FGF23 on phosphate excretion.[3,43,44] The ectodomain of klotho can be proteolytically cleaved, which generates a soluble fragment (soluble klotho [sKL]) that can be released from the kidney and detected in the circulation.[45–49] It was postulated that sKL functions as a hormone with pleiotropic, tissue-protective effects,[50,51] which acts independently of FGF23. CKD and aging are states of klotho deficiency,[52,53] and mice lacking klotho develop severe cardiovascular abnormalities, such as vascular calcification as well as cardiac hypertrophy and fibrosis.[2,13,54,55] Furthermore, klotho deficiency predisposes the heart to stress-induced cardiac injury.[56,57] Klotho is not expressed in cardiac myocytes,[2,13] and therefore a loss of transmembrane klotho cannot directly contribute to cardiac hypertrophy. Because in animal models of klotho deficiency, restoration of kidney klotho expression and of serum sKL levels ameliorates cardiovascular damage,[54,55,58] it is assumed that a reduction in sKL's direct protective effects on the cardiovascular system causes injury. However, experimental evidence indicating that sKL protects tissues by directly targeting them is still missing. It remains unclear whether pathologies associated with a global reduction in klotho expression are caused indirectly by the loss of transmembrane klotho in the kidney, resulting in systemic alterations, such as elevations in serum levels of phosphate or FGF23, or directly by the absence of sKL and its tissue protective actions. To date, an sKL receptor has not been identified and it remains unclear whether sKL can directly induce signal transduction and modulate effects in specific target cells such as cardiac myocytes.[59] It has been postulated that the direct cellular effects of sKL require intrinsic glycosidase activity[60–62] that modifies specific cell surface receptors organized in lipid rafts on various target cells.[63,64]

The recent analysis of the crystal structure revealed that FGF23, sKL, and FGFR1c form a complex, where sKL functions

as a nonenzymatic scaffold protein that brings FGFR1c and FGF23 in close proximity, thereby conferring stability of the ternary complex and promoting FGF23-mediated signaling.[65] This study suggests that sKL acts as an on-demand bona fide coreceptor for FGF23 and that the effects of sKL are FGF23 dependent, thereby challenging the concept that sKL can function as an FGF23-independent hormone. Surprisingly, this structural study also revealed the presence of HS in the FGF23/FGFR1c/sKL complex.[65] sKL and HS are part of the FGF23/FGFR signaling complex, and here we study the order of binding events among the different components. We determine whether sKL and HS function as independent FGF23 coreceptors and act on different FGFR isoforms, and we analyze whether both cofactors modulate the pathologic FGFR4-mediated actions of FGF23 on the heart.

METHODS

Plasmid constructs

Mouse soluble and full-length klotho and β-klotho cDNAs were kindly provided by Dr. Makoto Kuro-o (University of Texas Southwestern Medical Center, Dallas, TX),[43,66] and human soluble and full-length klotho cDNA constructs were from Amgen.[67] Inserts were subcloned into vectors with appropriate epitope tags, that is, C-terminal Strep/6xHis (OG1240, Oxford Genetics) or C-terminal FLAG/His (OG1232, Oxford Genetics). Subcloning was performed with appropriate restriction enzymes (New England Biolabs [NEB]) according to the manufacturer's protocols, and constructs were verified by Sanger sequencing. The EGFP-N1 vector used for green fluorescent protein (GFP) overexpression was from Clontech.

Antibodies, recombinant proteins, and heparin

Recombinant proteins from R&D Systems are human FGF2 (233-FB/CF), human FGF5 (237-F5/CF), human FGF7 (251-KG/CF), human FGF8b (423-F8/CF), human FGF19 (969FG025/CF), human FGF21 (2539FG025/CF), human FGF23 (2604FG025/CF), mouse FGF23 (2629FG025/CF), human FGFR1c (658FR050), human FGFR2c (712FR050), human FGFR3c (766FR050), and human FGFR4 (685FR050). The sKL recombinant protein produced by our laboratory is mouse aa 35-982 and human aa 34-981. Mouse sKL from R&D Systems (1819KL050) is aa 35-982; human klotho domain 1 (KL1) from PeproTech is aa 34-549. Heparin solution is from Celsus Laboratories for surface plasmon resonance experiments and from Pfizer Injectables for all other studies (NDC0069005902). Primary antibodies used are anti-FGF19 (AF969, R&D Systems), anti-FGF21 (AF2539, R&D Systems), anti-FGF23 (AF2604, R&D Systems), anti-FLAG (F1804, Sigma-Aldrich), anti-human crystallizable fragment (Fc; W4031, Promega), total extracellular signal–regulated kinase (ERK; 4695S, Cell Signaling), phosphorylated ERK (9101S, Cell Signaling), glyceraldehyde-3-phosphate dehydrogenase (GAPDH; CB1001, Millipore), and sarcomeric α-actinin (EA-53, Sigma-Aldrich). Secondary antibodies are horseradish peroxidase (HRP)–conjugated anti-goat (V8051, Promega), anti-mouse (W4021, Promega), and anti-rabbit (W4011, Promega) for Western blotting; HRP-coupled anti-human antibody (109035098, Jackson ImmunoResearch Laboratories) and anti-FLAG (A8592, Sigma-Aldrich) for the plate-based binding assay; and Cy3-conjugated goat–anti-mouse (115165166, Jackson ImmunoResearch Laboratories) for immunocytochemistry. We used anti-FGF23 antibody provided by Amgen to block FGF23 effects *in vitro*.[68]

Expression and purification of sKL

To overexpress and purify recombinant sKL protein, we used Expi-human embryonic kidney (HEK)293 cells (Expi293; A14527, Thermo Fisher Scientific) that were adapted to attached growth in Dulbecco's Modified Eagle's Medium (DMEM; 10013CV, Corning) supplemented with 10% fetal bovine serum (FBS; 26140079, Gibco) and 1× Penicillin-Streptomycin (Pen/Strep; 15140122, Gibco). Cells were transfected with appropriate klotho cDNA vectors using FuGENE 6 (E2691, Promega) in Opti-MEM (31985062, Gibco). After 2 days, clones were selected by using 1 μg/ml of puromycin (A1113803, Gibco). The clone with the highest expression was selected and readapted to suspension growth in Expi293 Expression Medium (A1435101, Thermo Fisher Scientific) supplemented with 1 μg/ml of puromycin and 1× Pen/Strep. Cells were grown in 250-ml shaker flasks with 100 ml of the medium on the MaxQ CO_2 plus shaker (88881101, Thermo Fisher Scientific) at 14*g*, 37 °C, and 5% CO_2. For protein production, cells were allowed to reach maximum density and collected via centrifugation at 400*g* and reseeded at densities of 1:100. Cells from 500 ml of the medium were pooled and lysed in 150 ml of radioimmunoprecipitation assay buffer (RIPA; 50 mM sodium phosphate [pH 7.5], 200 mM NaCl, 1% Triton X-100, 0.25% deoxycholic acid) with the addition of a protease inhibitor (11873580001, Roche) for 30 minutes. The mixture was then centrifuged at 20,000*g* for 1 hour to remove all cell debris, and the supernatant was sterile filtered for purification. Lysate was applied to a 5 ml TALON column (28953767, GE Healthcare) on the ÄKTA Start system (GE Healthcare) in running buffer containing 50 mM sodium phosphate and 300 mM NaCl. Elution was performed in running buffer supplemented with 200 mM imidazole.

For Strep-tagged sKL, fractions positive for sKL protein were diluted 1:2 in Buffer W (100 mM tris(hydroxymethyl)-aminomethane [Tris] [pH 8.0], 150 mM NaCl), captured on a 1-ml Strep-Tactin XT 4Flow column (24025001, IBA Lifesciences), and eluted with 100 mM biotin (BP2321, Fisher) in Buffer W. Positive fractions were collected, diluted 1:10 in 25 mM Tris (pH 8.0) running buffer, and applied to a 1 ml HiTrap Q HP column (29051325, GE Healthcare). The sample was eluted with running buffer in 500 mM NaCl, and sKL was aliquoted and flash frozen. The protein concentration was determined using Coomassie gel analysis in comparison to a bovine serum albumin (BSA) gradient.

For FLAG-tagged sKL, TALON column–positive fractions were diluted 1:10 in 10 mM Tris (pH 7.0) running buffer and applied to a 5 ml heparin column (17040701, GE Healthcare). The sample was eluted on a linear gradient of 0.0 to 1.0 M NaCl. Positive fractions for sKL were identified via our plate-based detection assay (detailed below) and pooled. The sample was diluted 1:10 and applied to a 1 ml HiTrap Q HP column (29051325, GE Healthcare) after TALON column purification. The sample was eluted with a 0.0 to 0.5 M NaCl gradient. Again, positive sKL fractions were identified by our klotho detection assay and flash frozen. The protein concentration was determined using Coomassie gel analysis in comparison to a BSA gradient.

FLAG immunoprecipitations

To study the interaction between FLAG-tagged sKL and different FGF isoforms, we conducted co-immunoprecipitation studies. FLAG beads (A2220, Sigma-Aldrich) were used at 50 μl of 50% stock slurry per sample. Beads were washed 5× with activity buffer (50 mM Tris [pH 7.4], 200 mM NaCl, 0.01% Tween 20, Sigma-Aldrich). Bead spin-down assays were all performed for 2 minutes at 5000*g*. Fifty microliters of a 50% slurry of beads per sample was

resuspended in 1 ml of activity buffer in a 1.5-ml snap cap tube. One microgram of FLAG-tagged sKL or Carboxy-terminal bacterial alkaline phosphatase (BAPC; P7457, Sigma-Aldrich) was incubated with the beads for 1 hour on a bead rotator. Beads were then pelleted at 5000*g* for 2 minutes and washed 5× with activity buffer. Beads were resuspended in 1 ml of activity buffer and samples with 500 ng of FGF. Beads were incubated for 1 hour on a tube rotator, and beads were pelleted and washed as before. One hundred microliters of 1× Laemmli sample buffer (1610737, Bio-Rad) with 1.42 M 2-mercaptoethanol was added, and samples were boiled for 5 minutes and analyzed using sodium dodecylsulfate–polyacrylamide gel electrophoresis (SDS-PAGE) and Western blotting, as described below.

Protein A/G immunoprecipitations

To study the interaction between Fc-tagged FGFR isoforms (Fc-FGFR), FGF isoforms, and sKL, we conducted immunoprecipitation studies. Protein A beads (6501, BioVision) and protein G beads (6511, BioVision) were used at 25 μl of a 50% stock slurry per sample in a total bead volume of 50 μl. Beads were washed 5× in activity buffer (50 mM Tris [pH 7.4], 200 mM NaCl, 0.01% Tween 20). Bead spin-down assays were all performed for 2 minutes at 5000*g*. Beads were resuspended in 1 ml of activity buffer in a 1.5-ml snap cap tube. One microgram of Fc-FGFR1 to 4 was incubated with the beads for 1 hour on a bead rotator. Control samples were incubated with 2 μg of anti-FGF antibody instead of Fc-FGFR. Beads were then pelleted at 5000*g* for 2 minutes and washed 5× with activity buffer. Beads were resuspended and incubated with different combinations of 500 ng of FGF, 1 μg of sKL, 1.6 United States Pharmacopeia (USP) units of heparin, or phosphate-buffered saline (PBS). Beads were incubated for 1 hour on a tube rotator, and beads were pelleted and washed as before. One hundred microliters of 1× Laemmli sample buffer (1610737, Bio-Rad) with 1.42 M 2-mercaptoethanol was added, and samples were boiled for 5 minutes. Samples were analyzed using SDS-PAGE and Western blotting.

SDS-PAGE and Western blotting

The sample (20 μl) was loaded onto Mini-PROTEAN TGX Precast Gel 4-20% for experiments with <9 samples (4568094, Bio-Rad) or Criterion TGX Precast Gel 4-20% (5678094, Bio-Rad) for experiments with >9 samples. Gels were run in 1× Tris/Glycine/SDS buffer (1610732, Bio-Rad) at 150 V and stopped when the sample dye reached the end of the gel. Gels were removed and electrotransferred via a semi-dry cassette (1703940, Bio-Rad) in 1× Tris/Glycine buffer (1610734, Bio-Rad) with 20% methanol. Gels were transferred onto polyvinylidene diflouride membranes (IPVH00010, Millipore) at 20 V for 1 hour. Membranes were then blocked in 5% dried milk with 0.5% Tween 20 diluted in Tris-buffered saline (TBST; pH 7.5) for 1 hour and probed with antibodies against specific antigens at 1:1000 in TBST with 5% dried milk. Blots were washed 3× for 5 minutes in TBST and probed with HRP-coupled secondary antibodies against specific species at 1:10,000 in TBST with 5% dried milk. Membranes were imaged on the SRX-101A X-ray film developer (Konica Minolta).

Paracrine FGF signaling in HEK293 cells

To determine the cellular activity of paracrine FGFs, we studied the activation/phosphorylation of ERK in HEK293 cells after treatment. HEK293 cells were seeded in 6-well plates in DMEM (26140079, Gibco) supplemented with 1× Pen/Strep (15140122, Gibco) and 10% FBS (26140079, Gibco) and grown for 48 hours. Upon reaching 80% confluence, cells were serum starved overnight in DMEM and 1× Pen/Strep without FBS. The medium was changed, and cells were treated with sKL at 2 μg/ml or vehicle (sKL elution buffer: 25 mM Tris ph 8.0, 500mM NaCl) for 15 minutes. Cells were then treated with various FGFs at 1.1 nM for 10 minutes. Cells were lysed in 200 μl of RIPA with the addition of a protease inhibitor (11836153001, Roche) and phosphatase inhibitors (P5726 and P0044, Sigma-Aldrich) for 30 minutes. The mixture was then centrifuged at 20,000*g* for 60 minutes to remove all cell debris. One hundred microliters of 1× Laemmli sample buffer (1610737, Bio-Rad) with 1.42 M 2-mercaptoethanol was added, and samples were boiled for 5 minutes. Twenty microliters of samples was loaded onto 12% SDS-PAGE gels and analyzed using Western blotting for total and phosphorylated ERK.

Plate-based assay to detect sKL and to study the paracrine FGF-sKL crosstalk

Proteins were coated on 96-well plates (MaxiSorp; 439454, Thermo Fisher Scientific), and proteins were added to wells in 100 μl of enzyme-linked immunosorbent assay (ELISA) coating buffer (E107, Bethyl Laboratories) with a lid placed overtop and incubated at 4 °C overnight. Plates were washed 5× with 350 μl of assay buffer (50 mM Tris [pH 7.4], 200 mM NaCl, 0.01% Tween 20) on a 50 TS microplate washer (BioTek). Plates were blocked for 1 hour in 200 μl of assay buffer with 0.5% BSA. Plates were washed as before, and proteins were incubated on plates in 100 μl of assay buffer with 0.5% BSA. Proteins or heparin was incubated in orders described in the respective figure legends. Assays using FLAG-tag–based detection were incubated with anti-FLAG coupled to HRP at 1:20,000, and assays using Fc detection were incubated with anti-human Fc coupled to HRP at 1:10,000. Plates were washed as above, and 100 μl of 3,3′,5,5′-tetramethylbenzidine (TMB) substrate (E102, Bethyl Laboratories) was added for 15 to 20 minutes until positive wells developed a dark blue color. Reactions were stopped with ELISA stop solution (E115, Bethyl Laboratories) and analyzed using the Synergy H1 plate reader (BioTek) at 450 nm wavelength. All samples were run in triplicates, and individual readouts are displayed on graphs. As a control to remove background absorbance values, wells were coated with an equal amount of BSA to match the amount of protein coated in experimental wells and treated the same as experimental wells. To study the effects of sKL on the binding between paracrine FGFs and FGFRs, plates were run as above except coated with paracrine FGFs. Fc-FGFR1 was preincubated with sKL or vehicle for 60 minutes, and then the combination was added to wells and the assay was run as before.

sKL half-life

To determine the half-life of recombinant sKL protein in the circulation, rats were injected with the Strep-tagged mouse sKL that was purified as described above. Each group consisted of 3 male Sprague Dawley rats (9 weeks of age and weighing ∼300 g). For injections and bleeding, rats were anesthetized with 2.5% isoflurane. For injections, a shielded i.v. catheter (BD Insyte Autoguard 0.7 × 19 mm, catalog no. 381412) was inserted into the lateral tail vein and flushed with 100 μl of isotonic saline (0.9%). One milliliter of purified sKL protein dissolved in isotonic saline (100 μg/kg) or isotonic saline was then injected, and the catheter was flushed again with 100 μl of isotonic saline. For bleeding, a shielded i.v. catheter was inserted into the lateral tail vein. Blood samples (300 μl) were taken after 1, 3, 5, 10, 15, 30, and 60 minutes as well as 3, 6, 12, and 48 hours. For collections from 15 minutes to 48 hours postinjection, a

separate i.v. catheter was inserted each time to draw blood. For collections from 1 to 15 minutes post-sKL injection, the same i.v. catheter was used, and to exclude contamination with the previous draw, the catheter was flushed with isotonic saline between each sample. Blood was collected into Multivette serum gel tubes (15.16.74, Sarstedt) and centrifuged at 10,000*g* for 5 minutes to purify serum. Serum was then aliquoted and stored at −80 °C before analysis. For the sKL activity assay, wells were coated with 500 ng of mouse FGF23 in 100 μl of coating buffer (E107, Bethyl Laboratories) at 4 °C overnight. Plates were washed 5× at 350 μl of assay buffer (50 mM Tris, [pH 7.4] 200 mM NaCl, 0.01% Tween 20) on a 50 TS microplate washer (BioTek). Plates were blocked for 1 hour in 200 μl of assay buffer with 0.5% BSA. Plates were washed and incubated with 30 μl per well and 70 μl of assay buffer with 0.5% BSA. Standards were run at noted concentrations by using our purified Strep-tagged mouse sKL protein with 30 μl of control serum and 70 μl of assay buffer with 0.5% BSA added to ensure consistency. All samples and standards were run in triplicates. After 1 hour, plates were washed, and 150 ng of Fc-FGFR1c were incubated on plates in 100 μl of assay buffer with 0.5% BSA. After 1 hour, plates were washed and incubated with anti-human Fc-HRP at 1:10,000. Plates were washed as above and 100 μl of TMB substrate (E102, Bethyl Laboratories) was added for 15 to 20 minutes until positive wells developed a dark blue color. Reactions were stopped with ELISA stop solution (E115, Bethyl Laboratories) and analyzed using the Synergy H1 plate reader (BioTek) at 450 nm wavelength. Amounts of sKL were calculated by taking the slope of the standard curve and calculating where the sample points fit in.

Plate-based sKL activity assay specificity test

HEK293 cells were plated in 10 cm dishes supplemented with 10% FBS (26140079, Gibco) and 1× Pen/Strep (15140122, Gibco). Cells were transfected with appropriate klotho or green fluorescent protein cDNA constructs. After 2 days, clones were selected by using 1 μg/ml of puromycin (A1113803, Gibco). Cells were then split and plated in 10 cm dishes in DMEM supplemented with FBS and puromycin. After 48 hours, cells were lysed in 1 ml of RIPA buffer with the addition of a protease inhibitor (11873580001, Roche) for 30 minutes. The mixture was then centrifuged at 20,000*g* for 1 hour to remove all cell debris. Activity assay was run as above in the sKL half-life study. Instead of serum, 20 μl of the indicated cell lysate was used and combined with 80 μl of activity assay buffer. All other conditions were as listed above and data displayed as absorbance after 15 to 20 minutes.

Surface plasmon resonance

For the direct quantitative analysis of label-free molecular interactions in real time, we conducted surface plasmon resonance studies using BIAcore T200 and T200 evaluation software (28975001, Cytiva). Sensor SA (BR100398) and CM5 chips (BR100399) were from Cytiva. For the preparation of heparin chips, heparin (2 mg) and amine-PEG3-Biotin (2 mg, 21347, Pierce) were dissolved in 200 μl of H_2O and 10 mg of $NaCNBH_3$ was added. The reaction mixture was heated at 70 °C for 24 hours; an additional 10 mg of $NaCNBH_3$ was added; and the reaction was heated at 70 °C for another 24 hours. After cooling to room temperature, the mixture was desalted with the spin column (3000 MWCO). Biotinylated heparin was collected, freeze dried, and used for chip preparation. Biotinylated heparin was immobilized to streptavidin chips according to the manufacturer's protocol. In brief, 20 μl of biotinylated heparin solution (0.1 mg/ml) in HBS-P running buffer (0.01 M *N*-2-hydroxyethylpiperazine-N′-2-ethanesulfonic acid, 0.15 M NaCl, 0.005% surfactant P20 [pH7.4]; BR100368, Cytiva) was injected over flow cell 2 of the streptavidin chip at a flow rate of 10 μl/min. The successful immobilization of heparin was confirmed by the observation of an ∼200-resonance unit increase in the sensor chip. The control flow cell (flow cell 1) was prepared by 1-minute injection with saturated biotin. For the preparation of FGFR4 chips, Fc-FGFR4 protein (human ectodomain) was immobilized on research grade CM5 chips according to the standard amine coupling protocol. Briefly, carboxymethyl groups on the CM5 chip surface were first activated using an injection pulse of 35 ml (flow rate 5 ml/min) of an equimolar mix of *N*-ethyl-*N*-(dimethylaminopropyl) carbodiimide and *N*-hydroxysuccinimide (final concentration 0.05 M, mixed immediately before injection). After activation, FGFR4 was diluted to 50 μg/ml in 100 mM sodium acetate (pH 5.5) buffer and injected over the activated biosensor surface. Excess unreacted sites on the sensor surface were deactivated with a 35 μl injection of 1 M ethanolamine. A reference flow cell was prepared using an injection pulse of 35 ml (flow rate 5 ml/min) of an equimolar mix of *N*-ethyl-*N*-(dimethylaminopropyl) carbodiimide and *N*-hydroxysuccinimide (final concentration 0.05 M, mixed immediately before injection) followed by a 35 μl injection of 1 M ethanolamine. For the measurement of interactions between FGF23 (human protein), FGFR4 (human ectodomain protein), klotho (human ectodomain, self-made; see above), and heparin, samples were diluted in HBS-P buffer. Different dilutions of protein were injected at a flow rate of 30 μl/min with HBS-P buffer as running buffer. At the end of the sample injection, HBS-P buffer was flowed over the sensor surface to facilitate dissociation. After a 3-minute dissociation time, the sensor surface was regenerated by injecting with 30 μl of 2 M NaCl to get a fully regenerated surface. The response was monitored as a function of time (sensorgram) at 25 °C.

Isolation and cultivation of neonatal rat ventricular myocytes

Neonatal rat ventricular myocytes (NRVMs) were isolated using a kit according to the manufacturer's protocol (LK003300, Worthington Biochemical Corporation), as done previously.[13,16,17] Briefly, hearts from 1- to 3-day-old Sprague Dawley rats (Envigo) were harvested and minced in calcium- and magnesium-free Hanks balanced salt solution and the tissue was digested with 50 μg/ml of trypsin at 4 °C for 20 to 24 hours. Soybean trypsin inhibitor in Hanks balanced salt solution was added, and the tissue was further digested with collagenase (in Leibovitz L-15 medium) under slow rotation (0.14*g*) at 37 °C for 45 minutes. Cells were broken up by triturating the suspension 20× with a standard 10-ml plastic serological pipette. Cells were then filtered through a cell strainer (70 μm, BD Falcon). Cells were incubated at room temperature for 20 minutes and spun at 100*g* for 5 minutes. The cell pellet was resuspended in plating medium (DMEM Base [10013CV, Corning], 17% M199 [12350039, Gibco], 15% FBS [26140079, Gibco], 1× Pen/Strep [15140122, Gibco]). For cell tracings, NRVMs were grown in 24-well plates on glass coverslips (CLS1760012, Chemglass). Slips were precoated with laminin (23017015, Invitrogen) at 10 μg/ml for 1 hour at 37 °C dissolved in PBS. Laminin was aspirated, and cells and medium were added. Cells were counted by a hemocytometer and plated at 4×10^5 cells per well. Myocytes were grown for 72 hours in the presence of plating medium; the medium was removed, and maintenance medium (DMEM Base [10013CV, Corning], 20% M199 [12350039, Gibco], 1% insulin-transferrin-sodium selenite solution [I18841VL, Sigma-Aldrich], 1× Pen/Strep [15140122, Gibco], 100 μM 5-bromo-2′-deoxyuridine [B9285, Sigma-Aldrich]) were added. After 48 hours,

maintenance medium was replaced, and after another 48 hours, cells were ready for treatment, giving a total of 72 hours of plating medium and 96 hours of maintenance medium before treatment. Cells were then treated for 48 hours.

Immunocytochemistry and morphometry of NRVMs

The medium was aspirated, and cultured NRVMs were fixed in 2% paraformaldehyde (P-6148, Sigma-Aldrich) and 4% sucrose dissolved in PBS for 5 minutes followed by permeabilization with 1% Triton X-100 dissolved in PBS for 10 minutes. Coverslips were washed 3× in PBS and blocked for 1 hour in blocking solution (2% FBS [26140079, Gibco], 2% BSA [BSA50, Rockland], 0.2% cold-water fish skin gelatin [900033, Aurion] dissolved in PBS). Blocking solution was aspirated, and 100 μl of 1:1000 α-actinin primary antibody was added for 1 hour. The primary antibody was aspirated, and coverslips were washed 3× with blocking solution and then 100 μl of Cy3-conjugated goat–anti-mouse secondary antibody diluted at 1:300 was added. After 1 hour, coverslips were washed 3× with blocking solution, dabbed dry, and mounted in ProLong™ Diamond Antifade Mountant with DAPI (P36962, Thermo Fisher Scientific) for visualization of nuclei. Immunofluorescence images were taken with a Leica DMi8 fluorescence microscope with a 63× oil immersion objective. The cross-sectional area of myocytes was measured on the basis of α-actinin–positive staining using ImageJ software (v1.53, National Institutes of Health). Each slide was from a different isolation to ensure reproducibility.

Adult rat ventricular myocyte isolation and analysis of calcium transients

As done before,[69] adult male Wistar rats (150–200 g) were killed and hearts were quickly removed and cannulated via the ascending aorta on a Langendorff system where they were retrograde perfused and digested by type II collagenase. Hearts were perfused with calcium-free Tyrode's solution supplemented with 0.2 mmol/l of ethyleneglycol-bis-(β-aminoethylether)-*N*,*N*,*N*',*N*'-tetraacetic acid for 3 minutes. For the digestion, hearts were perfused with Tyrode's solution containing 0.1 mmol/l of $CaCl_2$, 1 mg/ml of type II collagenase (Worthington), and 1 mg/ml of BSA for 3 to 4 minutes at room temperature. Cells were resuspended in Tyrode's solution containing 1 mmol/l of $CaCl_2$. Tyrode's solution contains 130 mM NaCl, 5.4 mM KCl, 0.4 mM NaH_2PO_4, 0.5 mM $MgCl_2$, 25 mM *N*-2-hydroxyethylpiperazine-*N*'-2-ethanesulfonic acid, and 22 mM glucose. Adult rat ventricular myocytes (ARVMs) were loaded with the fluorescent Ca^{2+} dye Fluo-3 AM (Thermo Fisher Scientific) for cytosolic Ca^{2+} measurements. Loaded ARVMs were acutely perfused during 2 minutes with vehicle, FGF23 (10 ng/ml), or a combination of FGF23 and heparin (0.7 USP/ml). Cytosolic Ca^{2+} transients were recorded under 1 Hz of field stimulation using 2 parallel platinum electrodes. Images were obtained with confocal microscopy (Zeiss LSM 510-META microscope), using a 40× objective by scanning the cell with an argon laser every 1.54 ms. Fluo-3 AM was excited at 488 nm, and emissions were collected at >505 nm. Cell contraction was stimulated as the difference in cell length between rest and contraction (during electrical stimulation), expressed as a percentage of shortening of the cell length. Image analysis was performed with self-made routines using IDL (Research Systems) and ImageJ (v1.53) software.

Isolated mouse heart contractility

Isolated heart contractility was performed as described previously.[14,70,71] Briefly, 2- to 3-month-old male CD-1 mice were anesthetized using 3% isoflurane and hearts were carefully removed and placed into oxygenated Ringer's solution composed of 140 mM NaCl, 2.0 mM KCl, 2.5 mM $CaCl_2$, 1.0 mM $MgSO_4$, 1.5 mM K_2HPO_4, 10 mM *N*-2-hydroxyethylpiperazine-*N*'-2-ethanesulfonic acid, and 10 mM glucose (pH 7.4). Atria were then removed, and the intact ventricular muscle was attached to small metallic clips hung vertically from a force transducer (ADInstruments) between bipolar platinum-stimulating electrodes and suspended in 25-ml glass tissue chambers (ADInstruments). Heart muscles were perfused with Ringer's solution continuously bubbled with 100% O_2 at room temperature. Hearts were stretched to the length of maximum force development and paced at 1 Hz (5 ms pulse duration, 30–60 V; Grass Instruments SD9 Square Pulse Stimulator). After a stable baseline was obtained, hearts were treated with either vehicle or FGF23 (9 ng/ml) alone or in combination with heparin (0.06 USP/ml) while contractile force output was monitored for 30 minutes. Contractile data were recorded and analyzed with LabChart 8 software (ADInstruments). Waveform changes were analyzed for peak contraction force (in millinewtons) and maximum slope of force development and presented as fold change from baseline values.

FGF23 serial injections

FGF23 injections were administered following a similar protocol established by us[13] and others.[72,73] Briefly, 12-week-old male BALB/c mice (The Jackson Laboratory) underwent tail vein injections. The day before the experiment, mice underwent echocardiographic analysis, as described below. Mice were anesthetized in 2.5% isoflurane and placed on a heat pad. Each group consisted of 5 mice, and different groups were injected with isotonic saline, heparin, FGF23, or FGF23 and heparin combined. Per injection, we used 40 μg/kg of FGF23 and 125, 62.5, or 12.5 USP/kg of heparin dissolved in 200 μl of isotonic saline, with 8 hours between injections for a total of 5 consecutive days. All injections were performed via the lateral tail vein. On the morning of the sixth day, 16 hours after the final tail vein injection, animals underwent echocardiographic analysis and were killed. Middle sections of hearts were cut along the short axis and stored overnight in 4% phosphate-buffered formaldehyde solution. Sections were sent to IDEXX Laboratories for embedding, hematoxylin and eosin (H&E) staining, and sectioning. Sections for wheat germ agglutinin (WGA) labeling were not stained by IDEXX Laboratories.

Adenine diet–administered mice

This diet-induced model of CKD, which develops kidney tubulointerstitial damage and cardiac hypertrophy, was constructed in accordance with previous studies.[74,75] We studied male and female mice in separate groups on the basis of the gender-specific effect of adenine, with females taking much longer (16–20 weeks) to develop kidney injury.[76] Five-week-old BALB/c mice (The Jackson Laboratory) were put on the control diet for 1 week. After 1 week, male and female mice were each split into 4 groups, receiving control chow and saline injections, control chow and heparin injections, adenine chow and saline injections, or adenine chow and heparin injections. Mice were administered an adenine diet (0.2% adenine, Teklad) or a control diet (same composition as adenine diet lacking adenine, Teklad) on the basis of their group and injected via the lateral tail vein with 125 USP/kg of heparin dissolved in isotonic saline or with isotonic saline as a vehicle control. Injections were administered 3 times per week, every Monday, Wednesday, and Friday, to mimic a

dialysis schedule. During injections, mice were briefly anesthetized with 2.5% isoflurane and the injection was administered in the lateral tail vein. After 10 weeks, mice were killed and samples prepared as described above.

Morphology, fluorescence microscopy, and morphometry of mouse and rat hearts

Short-axis heart sections were stained with H&E (IDEXX Laboratories) and used for representative images. Pictures were taken with a Leica Dmi8 fluorescence microscope. We measured the cross-sectional area of individual cardiac myocytes in paraffin-embedded short-axis sections. Paraffin-embedded sections underwent deparaffinization 2× for 5 minutes in Shandon Xylene Substitute (9990505, Thermo Fisher Scientific) and then rehydrated through a graded ethanol series (99%, 97%, 70%), 2× for 5 minutes each. Antigen retrieval was performed in a microwave for 15 minutes in 1× unmasking solution (H3300, Vector Laboratories). Slides were washed 3× for 5 minutes each in PBS and then incubated for 1 hour in blocking solution (1% BSA50 [Rockland], 0.1% cold-water fish skin gelatin [900033, Aurion], 0.1% Tween 20). Slides were washed 3× in PBS and then incubated in 10 μg/ml of 594-conjugate WGA (W11262, Thermo Fisher Scientific) for 1 hour. Slides were washed 3× with PBS and then mounted in ProLong™ Diamond Antifade Mountant (P36961, Thermo Fisher Scientific). Immunofluorescence images were taken with a Leica Dmi8 fluorescence microscope with a 60× oil objective. ImageJ software (National Institutes of Health) was used to quantify the cross-sectional area of 25 cells per field in 4 fields along the mid-chamber free wall on the basis of WGA-positive staining.

Echocardiography of mouse hearts

Echocardiographic analysis was performed on day 6 of the experiment for FGF23-injected mice by using the Vevo 770 or Vevo 3100 imaging system (FUJIFILM VisualSonics). Animals were anesthetized with 1.5% isoflurane, and normal body temperature was maintained using a rectal probe for temperature monitoring. For analysis, both B- and M-mode images were obtained in the short- and long-axis views. Correct positioning of the transducer was ensured using B-mode imaging in the long-axis view before switching to the short-axis view. Image analysis was performed using Vevo 770 Workstation and Vevo LAB software (FUJIFILM VisualSonics). Measurement and calculation definitions (including formulas) for B-mode are presented in Supplementary Tables S3 and S4.

Serum chemistry

At the end of the experiment, blood was collected from mice at the time of killing via cardiac puncture, transferred into Microvette serum gel tubes (20.1344, Sarstedt), and centrifuged at 10,000*g* for 5 minutes. Serum supernatants were collected and stored at −80 °C. Analyses of standard serum chemistry parameters were performed at IDEXX BioAnalytics (60406, kidney panel); serum blood urea nitrogen was measured using mass spectrometry at the Bioanalytical Core, School of Medicine, O'Brien Center for Acute Kidney Injury Research, University of Alabama at Birmingham.

Statistics

Values are expressed as mean ± SEM. Comparison between groups was performed using 1-way analysis of variance followed by a *post hoc* Tukey test (for all comparisons of ≥3 groups) or using 2-tailed *t* tests. A significance level of $P \leq 0.05$ was accepted as statistically significant. No statistical method but experience from previous publications was used to predetermine sample size. No formal randomization was used in any experiment. For *in vivo* experiments, animals were unbiasedly assigned into different treatment groups. Group allocation was not performed in a blinded manner. Whenever possible, experimenters were blinded to the groups (e.g., in immunofluorescence and immunohistochemistry experiments by hiding group designation and genotype of animals until after quantification and analysis).

Approval of animal studies

All animal protocols and experimental procedures for FGF23 injections in mice, adenine diet in mice, sKL half-life studies in rats, and NRVM isolations from newborn rats were approved by the Institutional Animal Care and Use Committee at the School of Medicine, University of Alabama at Birmingham. Heart isolations from mice for contractility studies were approved by the Institutional Animal Care and Use Committee at the University of Missouri-Kansas City. ARVM isolations from adult rats were approved by the Bioethical Committee Universidad Autónoma de Madrid and the General Direction of Agriculture and the Environment at the Environment Council of Madrid. All animals were maintained in temperature-controlled environments with a 12-hour light/dark cycle and allowed ad libitum access to food and water. All protocols adhered to the *Guide for Care and Use of Laboratory Animals* to minimize pain and suffering.

RESULTS

sKL promotes FGF23 binding to various FGFR isoforms

We tested whether FGF23 and sKL can bind each other in the absence of FGFR. We incubated immobilized FLAG-tagged sKL derived from transfected HEK293 cells with recombinant FGF23 protein, and we could coprecipitate FGF23, which was not detected when a FLAG-tagged control protein was immobilized (Figure 1a). In contrast, sKL did not bind FGF19 or FGF21 (Supplementary Figure S1A and B). Next, we developed a binding assay, where 96-well plates were coated with recombinant FGF23 protein, and sequentially incubated with FLAG-tagged sKL, anti-FLAG antibody, anti-Fc antibody coupled to HRP, and HRP substrate, followed by the analysis of chemiluminescence. sKL bound FGF23, which was not observed when wells were coated with other FGF isoforms (Figure 1b). We also tested whether sKL can bind FGFR in the absence of FGF23. We immobilized Fc-coupled FGFR ectodomains on protein A/G beads and incubated with FLAG-tagged sKL in the absence of FGF23. We could coprecipitate FLAG-sKL with FGFR1c and to a lower extent with FGFR4 but detected no sKL binding to FGFR2c or FGFR3c (Figure 1c). Our findings indicate that sKL can bind both FGF23 in the absence of FGFR as well as specific FGFR isoforms in the absence of FGF23. We coated plates with FGF23, or with Fc-coupled ectodomains of FGFR1c or FGFR4, and then sequentially added FLAG-tagged sKL, HRP-coupled anti-FLAG antibody, and HRP substrate to determine whether sKL preferentially binds FGF23 over FGFR. FLAG-sKL bound with highest affinity to FGFR1c and with similar affinities to FGF23 and FGFR4 (Figure 1d).

It has been shown that sKL binding to FGFRs not only enhances the affinity of FGFRs for FGF23 but concomitantly

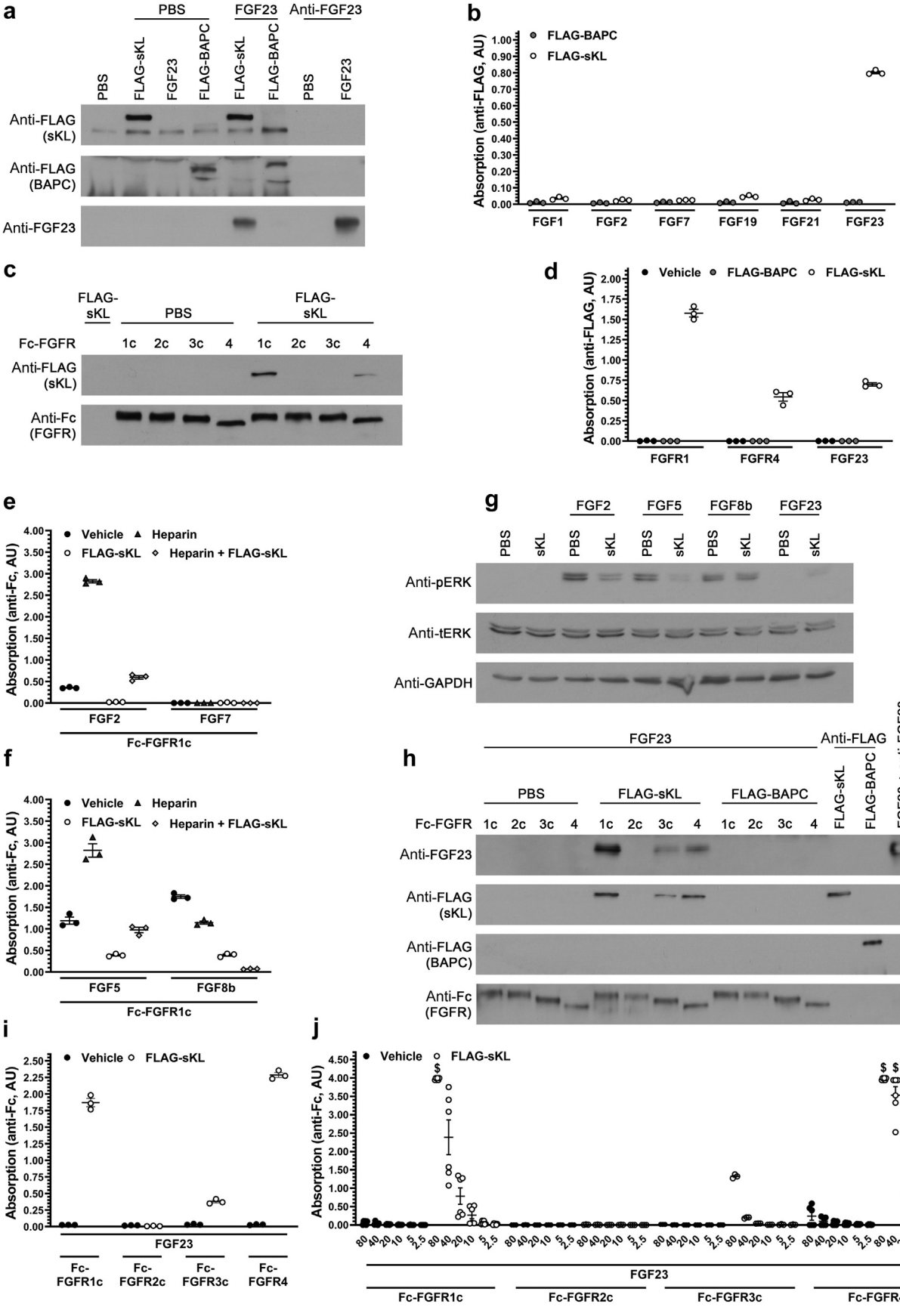
a
PBS
FGF23
Anti-FGF23
PBS
FLAG-sKL
FGF23
FLAG-BAPC
FLAG-sKL
FLAG-BAPC
PBS
FGF23
Anti-FLAG (sKL)
Anti-FLAG (BAPC)
Anti-FGF23
b
FLAG-BAPC
FLAG-sKL
Absorption (anti-FLAG, AU)
FGF1
FGF2
FGF7
FGF19
FGF21
FGF23
c
FLAG-sKL
PBS
FLAG-sKL
Fc-FGFR
1c 2c 3c 4 1c 2c 3c 4
Anti-FLAG (sKL)
Anti-Fc (FGFR)
d
Vehicle
FLAG-BAPC
FLAG-sKL
Absorption (anti-FLAG, AU)
FGFR1
FGFR4
FGF23
e
Vehicle
Heparin
FLAG-sKL
Heparin + FLAG-sKL
Absorption (anti-Fc, AU)
FGF2
FGF7
Fc-FGFR1c
f
Vehicle
Heparin
FLAG-sKL
Heparin + FLAG-sKL
Absorption (anti-Fc, AU)
FGF5
FGF8b
Fc-FGFR1c
g
FGF2
FGF5
FGF8b
FGF23
PBS sKL PBS sKL PBS sKL PBS sKL PBS sKL
Anti-pERK
Anti-tERK
Anti-GAPDH
h
FGF23
Anti-FLAG
PBS
FLAG-sKL
FLAG-BAPC
FLAG-sKL
FLAG-BAPC
FGF23 + anti-FGF23
Fc-FGFR 1c 2c 3c 4 1c 2c 3c 4 1c 2c 3c 4
Anti-FGF23
Anti-FLAG (sKL)
Anti-FLAG (BAPC)
Anti-Fc (FGFR)
i
Vehicle
FLAG-sKL
Absorption (anti-Fc, AU)
FGF23
Fc-FGFR1c
Fc-FGFR2c
Fc-FGFR3c
Fc-FGFR4
j
Vehicle
FLAG-sKL
Absorption (anti-Fc, AU)
80 40 20 10 5 2.5
FGF23
Fc-FGFR1c
Fc-FGFR2c
Fc-FGFR3c
Fc-FGFR4

suppresses FGFR binding to paracrine FGFs.[77] We used our plate-based binding assay to further test the hypothesis that sKL acts as an inhibitor of paracrine FGFs. Wells were coated with FGF2 or FGF7 and then sequentially incubated at the same molar concentrations with Fc-FGFR1 that had been preincubated with sKL, HRP-coupled anti-Fc antibody, and HRP substrate. In the absence of sKL, FGFR1c bound FGF2, but not FGF7 (Figure 1e), which is in line with previous studies showing that FGF7 prefers to interact with b splice isoforms of FGFRs.[77] Adding heparin before incubation with FGFR1c significantly increased FGF2 binding to FGFR1c. In contrast, heparin did not induce binding between FGF7 and FGFR1c. In the presence of FLAG-sKL, the binding of FGFR1c to FGF2 was significantly reduced. This inhibitory effect of sKL occurred in the absence and presence of heparin. Furthermore, sKL reduced the binding of FGFR1c to FGF5 and FGF8b (Figure 1f). To determine potential functional consequences of sKL's inhibitory actions toward paracrine FGFs, we coincubated HEK293 cells, which endogenously express various FGFR isoforms but lack klotho,[16] with FGFs and sKL. In the absence of sKL, paracrine FGF2, FGF5, and FGF8b induced ERK phosphorylation, indicating the activation of Ras/MAPK signaling, while endocrine FGF23 had no effect (Figure 1g). Coincubation with sKL decreased phospho-ERK levels in cells treated with FGF2 and FGF5, but induced ERK phosphorylation when cells were incubated with FGF23. Our findings suggest that while serving as a soluble coreceptor for FGF23 that mediates FGFR/Ras/MAPK signaling in the absence of endogenous membrane–associated klotho, sKL can block the klotho-independent activation of FGFR signaling induced by paracrine FGFs.

Next, we wanted to study whether the order of binding events—with sKL first binding to FGFR and second to FGF23 versus sKL first binding to FGF23 and second to FGFR—affects FGF23's affinity for FGFRs. We immobilized Fc-coupled FGFR ectodomains on protein A/G beads, followed by coincubation with FLAG-tagged sKL and FGF23. We found that FGFR1c, FGFR3c, and FGFR4 could coprecipitate sKL and FGF23 (Figure 1h). In contrast, we detected no FGF23 binding to any of the FGFR isoforms in the absence of sKL. Next, we coated plates with FGF23, followed by the sequential incubation with FLAG-tagged sKL, Fc-coupled FGFR ectodomains, HRP-coupled anti-Fc antibody, and HRP substrate. In the presence of sKL, FGF23 bound to FGFR1c, FGFR3c, and FGFR4 (Figure 1i), and these binding events occurred in a dose-dependent manner (Figure 1j). When the plate was coated with high amounts of FGF23, we also detected FGFR4 binding in the absence of sKL, which was not detected for the other FGFR isoforms (Figure 1j). Based on the sequential nature of the binding assay, FGF23 and sKL must have pre-formed before binding to FGFR ectodomains. As revealed by the pull-down as well as the plate binding assay, sKL did not mediate binding of FGF19 or FGF21 to any of the FGFR isoforms (Supplementary Figure S1C–E). Our findings indicate that sKL can increase FGFR binding affinity of FGF23 by doing both first binding to FGFR and serving as a soluble FGFR coreceptor or first binding

Figure 1 | Soluble klotho (sKL) modulates fibroblast growth factor receptor (FGFR) affinities of FGF23 and paracrine FGFs in an FGFR isoform–specific manner. (**a**) FLAG-tagged sKL or C-terminal bacterial alkaline phosphatase (BAPC) (used as a negative control) was immobilized on anti-FLAG beads and then incubated with recombinant FGF23 protein or solvent (phosphate-buffered saline [PBS]). Protein A/G beads with immobilized anti-FGF23 antibody and incubated with FGF23 served as a positive control for FGF23 precipitation. FLAG-sKL, but not FLAG-BAPC, bound FGF23. (**b**) 96-well plates (Thermo Fisher Scientific) were coated with 10 ng of recombinant FGF1, FGF2, FGF7, FGF19, FGF21, or FGF23, washed, and incubated with 40 ng of FLAG-tagged sKL or BAPC. After subsequent washes and incubation with horseradish peroxidase (HRP)–coupled anti-FLAG antibody and HRP substrate, absorbance at 450 nm was measured (presented as arbitrary units [AUs]). Of all the tested FGF isoforms, only FGF23 bound FLAG-sKL. (**c**) Crystallizable fragment (Fc)–tagged FGFR isoforms 1c, 2c, 3c, and 4 were bound to protein A/G beads and treated with either FLAG-tagged sKL or PBS. FLAG-sKL bound to FGFR4 and to a lower extent to FGFR4. (**d**) 96-well plates were coated with 40 ng of FGFR1c or FGFR4 or with 20 ng of FGF23, washed, and incubated with 80 ng of FLAG-tagged sKL or BAPC or PBS. Wells were washed again, treated with HRP-coupled anti-FLAG antibody and HRP substrate, and analyzed for absorbance at 450 nm. FLAG-sKL bound FGFR1c and to a lower extent FGFR4 and FGF23. (**e,f**) 96-well plates were coated with (**e**) 12.5 ng of FGF2 or FGF7 or (**f**) 100 ng of FGF5 or FGF8b and incubated with 0.4 United States Pharmacopeia (USP) units of heparin or PBS (vehicle). Wells were washed, incubated with 25 ng (for FGF2 and FGF7) or 200 ng (for FGF5 and FGF8b) of Fc-FGFR1c, washed again, and treated with HRP-coupled anti-Fc antibody and HRP substrate, followed by the analysis of absorbance at 450 nm. In reactions receiving sKL, Fc-FGFR1c was preincubated with 50 ng (for FGF2 and FGF7) or 400 ng (for FGF5 and FGF8b) of FLAG-tagged sKL before addition to wells. Heparin increased the binding of FGF2 and FGF5 to FGFR1c, but this effect did not occur in the presence of sKL. (**g**) Serum-starved human embryonic kidney 293T (HEK293T) cells were treated with sKL or PBS for 15 minutes, followed by stimulation with FGF2, FGF5, FGF8b, or FGF23 for 10 minutes. Total protein extracts were analyzed using Western blotting. Treatment with FGF2, FGF5, and FGF8b increased levels of phosphorylated extracellular signal–regulated kinase (pERK) in comparison to total levels of ERK (tERK), which did not occur if cells were pretreated with sKL. In contrast, FGF23 treatment increased pERK levels in the presence of sKL. Glyceraldehyde-3-phosphate dehydrogenase (GAPDH) served as a loading control. (**h**) One microgram of Fc-tagged FGFR isoforms 1c, 2c, 3c, or 4 was bound to protein A/G beads and treated with either 2 μg of FLAG-tagged sKL or BAPC or PBS, all in combination with 500 ng of FGF23. Anti-FLAG beads incubated with either FLAG-sKL or FLAG-BAPC, and anti-FGF23 antibody immobilized on protein A/G beads and treated with FGF23 served as positive controls for FLAG and FGF23 precipitations, respectively. Cotreatments with FGF23 and sKL led to complex formation with FGFR1c and to a lesser extent with FGFR3c and FGFR4. (**i**) 96-well plates (Thermo Fisher Scientific) were coated with 4.5 ng of FGF23, washed, and then sequentially incubated with 18 ng of FLAG-tagged sKL or PBS and 50 ng of Fc-tagged FGFR1c, 2c, 3c, or 4, HRP-coupled anti-Fc antibody, and HRP substrate, followed by absorbance measurement. The complex of FGF23 and sKL bound FGFR1 and FGFR4 the strongest, with weaker binding to FGFR3. (**j**) 96-well plates were coated with 2-fold dilutions of FGF23, ranging from 80 to 2.5 ng. Wells were washed and sequentially incubated with 320 to 10 ng of FLAG-tagged sKL or PBS, followed by 160 to 5 ng of Fc-FGFR1c, 2c, 3c, or 4, HRP-coupled anti-Fc antibody, and HRP substrate. Binding of the sKL/FGFR1c, sKL/FGFR3c, and sKL/FGFR4 complexes occurred in relation to the amount of coated FGF23. In the absence of sKL, FGF23 bound FGFR4 with weak affinity, but not FGFR1c, 2c, or 3c. All values are expressed as mean ± SEM. For plate-based assays, $n = 3$ replicate wells. [$]The absorbance at 450 nm surpassed the plate reader limit.

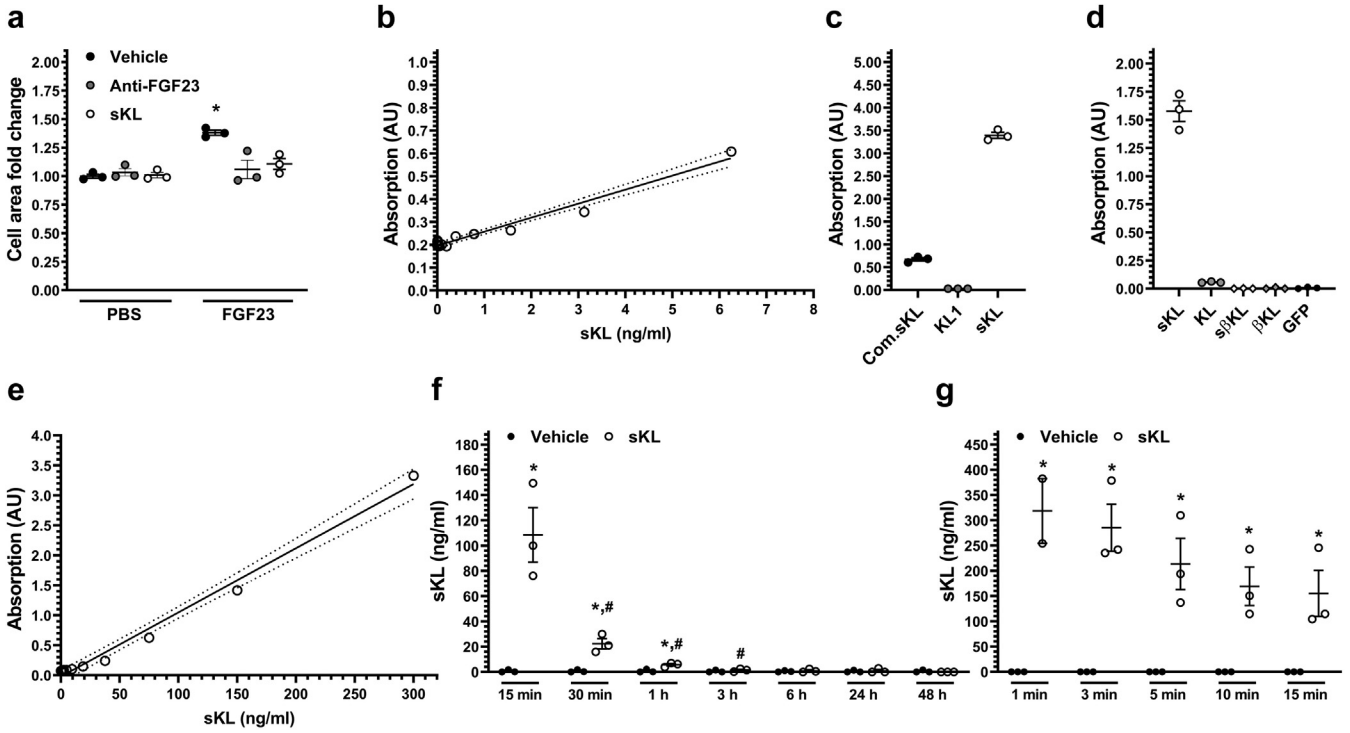

Figure 2 | Production and detection of bioactive soluble klotho (sKL), a fibroblast growth factor (FGF) 23 binding protein with antihypertrophic effects. (**a**) Neonatal rat ventricular myocytes were cotreated with FGF23 (25 ng/ml) or vehicle (phosphate-buffered saline [PBS]) and with sKL (100 ng/ml), anti-FGF23 blocking antibody (1 μg/ml), or vehicle. FGF23 treatments caused an increase in cell area, while sKL and anti-FGF23 blocked this effect. (**b,e**) Standard curves (linear regression) for the measurements of sKL using our plate-based assay, with FGF23 coated on 96-well plates (Thermo Fisher Scientific) and incubation with Fc-FGFR1c, followed by horseradish peroxidase (HRP)–coupled anti-Fc antibody and HRP for detection. sKL was applied in (**b**) assay buffer or (**e**) in rat serum as a diluent. For sKL in buffer, the assay gives a linear range allowing the calculation of sKL concentrations in samples with a limit of detection (LOD) of ∼300 pg/ml. For sKL in serum, the assay is ∼10× less sensitive, with an LOD of ∼10 ng/ml. Absorbances measured are depicted in arbitrary units (AUs) as individual dots and standard curves as straight lines. (**c**) Two commonly used commercial preparations of sKL (Com.sKL) and of the first extracellular domain of klotho (KL1) were analyzed in our sKL detection assay in comparison to our own sKL. Our sKL protein showed ∼7× higher binding activity than did Com.sKL, and we detected no binding of KL1. (**d**) Using our FGF23/Fc-FGFR1c–based detection assay, we analyzed binding affinities of different variants and isoforms of klotho, that is, sKL and full-length klotho (KL), as well as soluble β-klotho (sβKL) and full-length β-klotho (βKL). Human embryonic kidney 293T (HEK293T) cells were stably transfected with klotho constructs or a green fluorescent protein (GFP) vector used as a negative control, and total cell lysates were analyzed. A strong signal was observed for sKL and much weaker binding for KL. GFP, sβKL, and βKL showed no measurable binding activity. (**f**) Rats were injected via the tail vein with sKL (100 μg/kg) or vehicle (PBS), and serial bleeds were taken at different time points and analyzed by our FGF23/Fc-FGFR1c–based detection assay. At the 15-minute time point, high levels of sKL were detected in sKL-injected rats compared with vehicle-injected controls. sKL exhibited a half-life of <15 minutes, and starting at 3 hours postinjection, we could no longer detect sKL. (**g**) Rats were injected with sKL or vehicle as before, but serial bleeds were taken at earlier time points. After ∼10 minutes postinjection, sKL levels were reduced by about half. Comparison between groups was performed using 1-way analysis of variance followed by a *post hoc* Tukey test (**a**) or using 2-tailed *t* tests (**f,g**). A significance level of $P \leq 0.05$ was accepted as statistically significant. (**a**) $n = 3$ independent isolations, 50 cells per slide, 150 total cells per condition. $^{*}P \leq 0.05$ versus all other groups. (**c,d**) $n = 3$. (**f,g**) $n = 3$. $^{*}P \leq 0.05$ versus vehicle treated at the same time point, $^{\#}P \leq 0.05$ versus same treatment in the preceding time point. For plate-based assays, $n = 3$ replicate wells.

to FGF23 and serving as a circulating FGF23 binding partner. Either way, sKL mediates FGF23-FGFR binding in an FGFR isoform–specific manner, with highest FGF23-sKL affinities for FGFR1c and FGFR4, lower affinity for FGFR3c, and no binding to FGFR2c. Furthermore, in the absence of sKL, FGF23 can bind FGFR4 with low affinity, supporting the FGFR4-mediated actions of FGF23 elevations that have been reported in cells lacking klotho.[15,16]

sKL alleviates the cardiac effects of FGF23

Several studies have shown that elevated sKL levels in animal models of CKD have cardioprotective effects.[54,56,58,78,79] A recent study suggests that these effects are independent of sKL's antihypertensive effects and are rather based on the direct actions of sKL on the heart.[80] To determine whether sKL interferes with the direct effects of FGF23 on cardiac myocytes, we treated isolated NRVMs with FGF23 for 48 hours, which induced hypertrophic growth as determined by an increase in the area of immunolabeled cells (Figure 2a), as shown before.[13,16,17] When NRVMs were cotreated with sKL, FGF23 did not induce hypertrophy, similar to the inhibitory actions observed in the presence of anti-FGF23 blocking antibody. Treatment with sKL by itself had no effect on the NRVM area. Our finding is in line with our previous studies

showing that FGF23 treatment of isolated adult ventricular cardiac myocytes causes calcium mishandling, alters contractility, and triggers proarrhythmic calcium release, which can be blocked by sKL.[69] Furthermore, we found that administration of sKL protects a mouse model of CKD from developing ventricular arrhythmias.[79] Combined, these studies indicate that sKL can directly inhibit the pathologic actions of FGF23 on cardiac myocytes, suggesting the potential for sKL administration as a novel cardioprotective therapy that might be effective in scenarios of systemic FGF23 elevations, such as CKD. However, attempts from various groups to purify sKL protein in larger amounts have failed, and sKL protein appears to be highly unstable. The structural analysis of the klotho complex revealed the presence of a Zn^{2+} ion located in the linker region between the extracellular KL1 and KL2 domains, which is crucial for stabilizing klotho's elongated structure, for forming the FGF23 binding pocket, and for FGF23-induced Ras/MAPK signaling.[65] We have developed a novel procedure to synthesize and purify recombinant mouse and human sKL protein from stably transfected HEK293 cells in the absence of chelating agents, such as ethylenediamine tetraacetic acid (EDTA) and avoiding nonphysiological elution conditions (Supplementary Figure S2A). Because the function of sKL has been unknown, an assay to test the bioactivity of sKL is currently unavailable. On the basis of our finding that sKL can bind the ectodomain of different FGFR isoforms, with high binding affinity for FGFR1c, we have developed an assay that can detect biologically active sKL by its ability to sequentially bind FGF23 and FGFR1c (Supplementary Figure S3). We found that the assay can detect our self-made sKL protein dissolved in physiologic buffer in a concentration-dependent manner, with a limit for linear detection in the range of 300 pg/ml (Figure 2b). We used our assay to test the bioactivity of 2 commercially available sKL variants that have been used in various functional *in vitro* and *in vivo* studies.[54,78] The first variant contained the ectodomain of klotho and showed significantly reduced binding as compared with our sKL protein (Figure 2c), suggesting lower bioactivity. Because commercial sKL is stored in EDTA-based buffer, it is likely that the Zn^{2+} ion has been depleted, leading to structural changes and reduced activity of sKL. The second variant contained only the KL1 domain of klotho. Our plate-based binding assay revealed that KL1 cannot mediate FGF23-FGFR1c binding and therefore lacks biological activity, at least activity that is mediated by FGF23 and FGFRs (Figure 2c). This is in line with the recent structural study showing that sKL binding to FGF23 and FGFR1c is mediated by KL2 and the linker region connecting KL2 with KL1 but not by KL1.[65] Our assay also detected sKL in protein extracts derived from HEK293 cells overexpressing sKL (Figure 2d). Extracts from HEK293 cells overexpressing full-length klotho were negative in the detection assay, most likely on the basis of the unspecific accumulation of the transmembrane protein and thereby loss of bioactivity. Furthermore, the assay did not detect the transmembrane or soluble forms of β-klotho, indicating the specificity of the FGF23-FGFR detection assay for sKL (Figure 2d).

Although klotho expression in the kidney seems to be uniformly reduced in CKD, reported circulating levels of sKL in humans are extremely variable.[81] Inconsistent results in sKL measurements are probably due to ELISA-related variance.[82] Thus, a reliable assay to detect sKL is needed to fully assess the potential of sKL as a clinical biomarker. To test whether our FGF23-FGFR1c binding assay could detect sKL in serum, we administered our self-made murine sKL protein to rats by i.v. injection and we could detect sKL down to a concentration of 10 ng/ml (Figure 2e). Serial bleeds post-injection over time revealed a half-life in the circulation of ∼10 minutes for our recombinant sKL protein (Figure 2f and g). Elevations in circulating sKL levels were accompanied by increases in serum concentrations of FGF23 while phosphate levels were not altered (Supplementary Figure S2B and C). Combined, our procedure to detect sKL provides a novel assay that specifically detects sKL in its bioactive form, defined by its ability to increase the binding affinity of FGF23 for FGFR1c, in cell extracts and in rodent blood. Furthermore, by modifying the sKL synthesis procedure, we produced recombinant sKL protein with high bioactivity that could be used for preclinical studies in animal models.

Heparin increases the affinity of FGF23 for FGFR4

On the basis of the presence of HS in the FGF23/FGFR1c/sKL complex,[65] we wanted to determine whether HS can mediate FGF23/FGFR binding in the absence of sKL and thereby serve as an independent cofactor for FGF23/FGFR binding as established for FGFR binding of paracrine FGFs. We used heparin, a linear glycosaminoglycan structurally similar to HS, but with a higher degree of sulfation, that is used as an experimental proxy for HS. We immobilized Fc-coupled FGFR ectodomains on protein A/G beads, followed by coincubation with heparin and FGF23. We found that FGFR4 efficiently coprecipitates FGF23, and we also detected weaker FGF23 binding to FGFR1c, FGFR2c, and FGFR3c (Figure 3a). In contrast, we detected no FGF23 binding to any of the FGFR isoforms in the absence of heparin. FGFR4 showed the strongest FGF23 binding in the presence of heparin, which was still below the binding affinity that we detected when sKL was used instead of heparin. Next, we coated plates with FGF23, followed by the sequential incubation with heparin, Fc-coupled FGFR ectodomains, HRP-coupled anti-Fc antibody, and HRP substrate. In the presence of heparin, FGF23 bound to FGFR4 and to a much lesser extent to FGFR2c (Figure 3b), which occurred in a dose-dependent manner (Figure 3c). As observed before, FGF23 bound FGFR4 in the absence of heparin in a dose-dependent manner and the affinity of FGF23 for FGFR4 was significantly increased by heparin (Figure 3c). We detected no binding between FGF23 and FGFR1c or FGFR3c in the presence or absence of heparin (Figure 3c). Overall, our study suggests that in the absence of klotho, heparin can mediate the interaction between FGF23 and FGFRs. In contrast to FGF23, our co-immunoprecipitation and plate-based binding studies

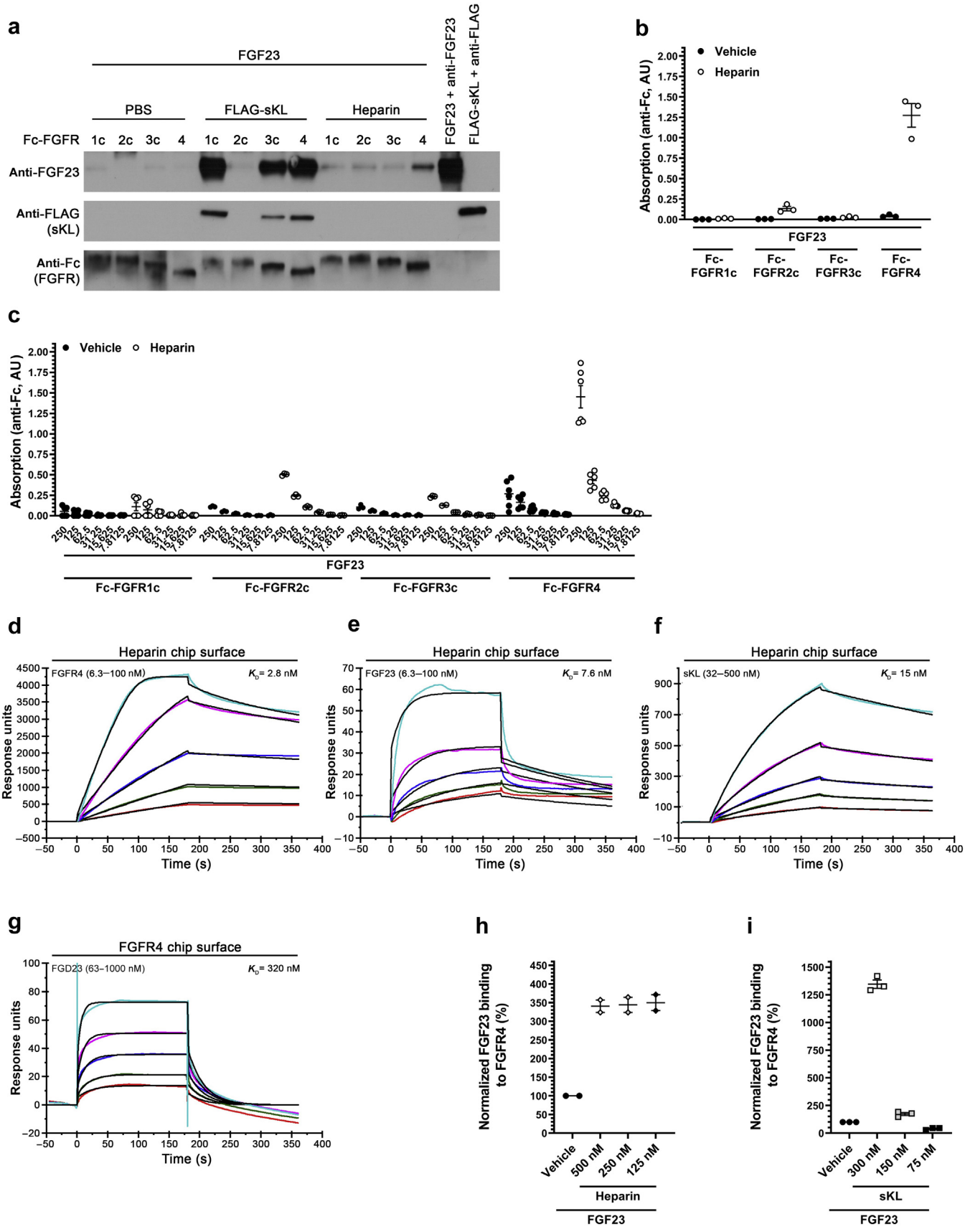

Figure 3 | Heparin can bind fibroblast growth factor receptor isoform 4 (FGFR4), klotho, and FGF23 and increases the affinity of FGF23 for FGFR4. (**a**) Crystallizable fragment (Fc)–tagged FGFR1c, 2c, 3c, and 4 were bound to protein A/G beads and treated with FGF23 (continued)

showed that heparin does not mediate binding of FGF19 or FGF21 to any of the FGFR isoforms (Supplementary Figure S1C–E).

We performed surface plasmon resonance analyses with heparin immobilized on a chip and purified soluble proteins to study which component of the FGF23/FGFR4/klotho complex could be directly bound by heparin and to determine precise binding affinities (Figure 3d–f; Supplementary Table S5). As expected,[83,84] we detected that heparin could bind FGFR4 with high affinity (dissociation constant K_D = 2.8 nM). Surprisingly, we found that heparin can also bind FGF23 and klotho with similar affinities (K_D = 7.6 nM and K_D = 15 nM, respectively). These findings suggest that heparin can independently bind FGFR4, klotho, and FGF23 with high affinity. Next, we studied the direct interaction between the immobilized ectodomain of FGFR4 and FGF23 (Figure 3g; Supplementary Table S5) and we detected low affinity binding (K_D = 320 nM), similar to other surface plasmon resonance studies[85] and in accordance with the low affinity binding detected by our plate-based assay (Figures 1j and 3c). When we conducted the FGF23/FGFR4 binding study in the presence of heparin, we detected an increase in binding affinity by ~3-fold (Figure 3h). When we repeated the study with sKL instead of heparin, FGF23/FGFR4 binding affinity increased by ~13-fold (Figure 3i). Combined, these findings indicate that heparin and sKL both can act as independent coreceptors that mediate FGF23/FGFR4 binding, whereby sKL's effect on increasing FGFR4 affinity for FGF23 is ~4- to 5-fold higher than that of heparin.

Heparin aggravates the cardiac effects of FGF23

Because we found that heparin mainly facilitates FGF23 binding to FGFR4, and it is known that the prohypertrophic actions of FGF23 on cardiac myocytes are mediated by FGFR4,[16,17,73] we wanted to determine whether heparin aggravates the cardiac effects of FGF23. First, we cotreated NRVMs with increasing concentrations of FGF23 and with heparin for 48 hours. We found that the gradual FGF23-induced increase in the cell area was further elevated in the presence of heparin (Figure 4a). Treatment with heparin by itself had no effect on the NRVM area. Because FGF23 alters calcium handling and contractility in isolated ARVMs,[69] we studied the potential effects of heparin in this context. Perfusion of ARVMs with FGF23 for 2 minutes increased systolic $[Ca^{2+}]_i$ transients, and this effect became statistically significant when cells were coperfused with FGF23 and heparin (Figure 4b and c). Furthermore, FGF23 increased cell contraction of ARVMs, which was significantly increased when cells were coperfused with FGF23 and heparin (Figure 4d). In both ARVM studies, heparin by itself had no significant effects. We have previously shown that the treatment of isolated adult mouse hearts with FGF23 for 30 minutes results in an increase in ventricular contraction as well as intracellular calcium.[14] This acute FGF23 effect occurs in a concentration-dependent manner and is mediated by FGFR4.[17] To determine whether heparin modulates FGF23's actions on cardiac contractility, we analyzed the contractile responses of isolated hearts from mice in the presence of FGF23 and heparin. Treatment with FGF23 increased cardiac contractile force compared with vehicle as previously reported.[14,17,71] When FGF23 was coincubated with heparin before addition to the organ bath, we detected a further increase in cardiac contractility force (Figure 4e and f). Combined, these findings suggest that heparin promotes the acute effects of FGF23 on the heart and further increases contractility properties and handling of intracellular calcium in cardiac myocytes and thereby might enhance calcium-dependent prohypertrophic signaling and calcium overload and trigger cardiac arrhythmogenicity.

Finally, we wanted to determine whether heparin aggravates the cardiac effects of FGF23 *in vivo*. First, we coinjected FGF23 and heparin in mice. We have shown before that 2 tail vein injections of recombinant FGF23 protein for 5 consecutive days induces cardiac hypertrophy,[13] which has been confirmed by others.[72,86,87] This effect requires the presence of FGFR4 in cardiac myocytes and occurs independently of

Figure 3 | (continued) in combination with either FLAG-tagged soluble klotho (sKL), heparin, or phosphate-buffered saline (PBS). Anti-FLAG beads incubated with FLAG-sKL and anti-FGF23 antibody immobilized on protein A/G beads and treated with FGF23 served as positive controls for FLAG and FGF23 precipitations, respectively. Cotreatments with FGF23 and sKL lead to complex formation with FGFR1c and to a lesser extent with FGFR3c and FGFR4. Cotreatment with heparin increased binding of FGF23 to FGFR4 and to a much lesser extent to the other FGFR isoforms. (**b**) 96-well plates (Thermo Fisher Scientific) were coated with 250 ng of FGF23, washed, and then sequentially incubated with 0.4 United States Pharmacopeia (USP) units of heparin or vehicle (PBS) and 500 ng of Fc-tagged FGFR1c, 2c, 3c, or 4, horseradish peroxidase (HRP)–coupled anti-Fc, and HRP substrate, followed by absorbance measurement. In the presence of heparin, FGF23 bound FGFR4 the strongest, with weaker binding to FGFR2c and no measurable binding to FGFR1c and FGFR3c. (**c**) 96-well plates were coated with 2-fold dilutions of FGF23, ranging from 250 to 7.8125 ng. Wells were washed and sequentially incubated with 0.4 USP of heparin or vehicle (PBS), followed by 500 to 15.625 ng of Fc-FGFR1c, 2c, 3c, or 4, HRP-coupled anti-Fc antibody, and HRP substrate. In the presence of heparin, FGF23 did not bind to FGFR1c or 3c, and binding of the heparin/FGFR4 and heparin/FGFR2c complexes occurred in relation to the amount of coated FGF23. In the absence of heparin, FGF23 bound FGFR4 with weak affinity, but not FGFR1c, 2c, or 3c. (**d**) Surface plasmon resonance (SPR) sensorgrams of the FGFR4-heparin interaction. Concentrations of FGFR4 (from top to bottom): 100, 500, 25, 12.5, and 6.3 nM, respectively. The black curves are the fitting curves using model from T200 evaluation software (version 3.2). The biosensor chip response is indicated on the *y* axis as a function of time (*x* axis). (**e**) SPR sensorgrams of the FGF23-heparin interaction. Concentrations of FGF23 (from top to bottom): 100, 500, 25, 12.5, and 6.3 nM, respectively. (**f**) SPR sensorgrams of the klotho-heparin interaction. Concentrations of sKL (from top to bottom): 500, 250, 125, 63, and 32 nM, respectively. (**g**) SPR sensorgrams of the FGF23-FGFR4 interaction. Concentrations of FGF23 (from top to bottom): 1000, 500, 250, 125, and 63 nM respectively. (**h**) Bar graphs based on triplicate experiments with standard deviation, showing normalized FGF23 binding to surface FGFR4 with the addition of different concentrations of heparin in solution. (**i**) Bar graphs based on triplicate experiments with standard deviation, showing normalized FGF23 binding to surface FGFR4 with the addition of different concentrations of sKL in solution.

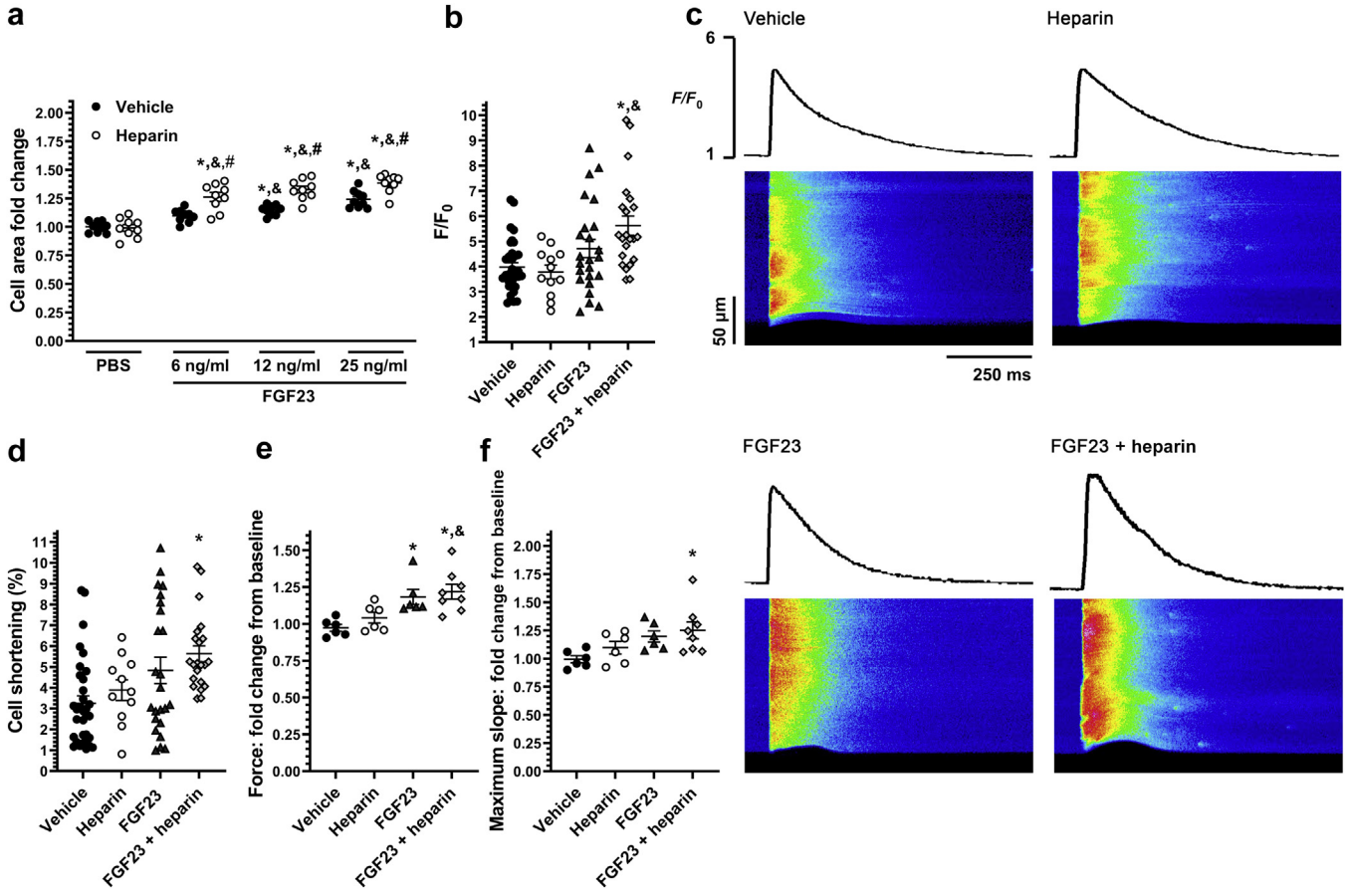

Figure 4 | Heparin promotes fibroblast growth factor (FGF) 23's prohypertrophic effects in cultured cardiac myocytes. (**a**) Neonatal rat ventricular myocytes were cotreated with FGF23 at indicated concentrations or vehicle (phosphate-buffered saline [PBS]) and with heparin (0.19 United States Pharmacopeia units [USP]/ml) or vehicle. FGF23 treatments caused a stepwise elevation in the cell area with increasing FGF23 concentrations. Heparin increased this effect at all FGF23 concentrations. (**b**) Adult rat ventricular myocytes (ARVMs) were treated with FGF23 (10 ng/ml), heparin (0.7 USP/ml), or a combination of both, and peak fluorescence $[Ca^{2+}]_i$ transients (F/F_0) were measured. FGF23 increased $[Ca^{2+}]_i$, and this change significantly increased in the presence of heparin. (**c**) Representative line scan images of ARVMs under 1 Hz field stimulation perfused with vehicle, heparin, FGF23, or FGF23 combined with heparin for the analysis shown in (**e**). (**d**) ARVMs were treated with FGF23, heparin, or a combination of both, and cell shortening after perfusion was measured. The addition of heparin significantly increased the effect of FGF23. (**e**) Intact hearts were isolated from adult mice, attached to a force transducer, paced, and treated with either vehicle, heparin (0.06 USP/ml), FGF23 (9 ng/ml), or a combination of FGF23 and heparin while contractile output was monitored. Waveform changes were analyzed for peak contraction force. FGF23 increased force, which was further elevated in the presence of heparin. (**f**) FGF23 with heparin also increased the maximum slope of force development of the contractile waveform. Comparison between groups was performed using 1-way analysis of variance followed by a *post hoc* Tukey test (**a,b,d–f**). A significance level of $P < 0.05$ was accepted as statistically significant. (**a**) $n = 9$. $^{*}P \leq 0.05$ versus PBS/PBS, $^{\&}P \leq 0.05$ versus PBS/heparin; $^{\#}P \leq 0.05$ versus FGF23 + vehicle at same concentrations. (**b,d**) $n = 5$, $n = 34$ (vehicle); $n = 3$, $n = 12$ (heparin); $n = 5$, $n = 24$ (FGF23); $n = 4$, $n = 22$ (FGF23 + heparin). $^{*}P \leq 0.05$ versus vehicle, $^{\&}P \leq 0.05$ versus heparin. (**e,f**) $n = 6$ (vehicle), $n = 6$ (heparin), $n = 6$ (FGF23), $n = 8$ (FGF23 + heparin). $^{*}P \leq 0.05$ versus vehicle, $^{\&}P \leq 0.05$ versus heparin. All values are expressed as mean ± SEM. For plate-based assays, $n = 3$ replicate wells.

blood pressure elevations,[73] suggesting that this is a mouse model of cardiac hypertrophy caused by the direct FGFR4-mediated actions of circulating FGF23 on the heart. Following the same protocol, we injected male BALB/c mice with 40 µg/kg of FGF23 and 125 USP/kg of heparin separately and together. Compared with vehicle and FGF23 injections, mice receiving FGF23 and heparin combined developed a significant increase in left ventricular wall thickness and left ventricular mass, as revealed by echocardiography (Figure 5a and b; Supplementary Figure S4A and Supplementary Table S1), resulting in an increase in the ratio of heart weight to tibia length (Figure 5c) and histological changes (Figure 5d). The increase in cardiac mass was not accompanied by changes in cardiac function, such as ejection fraction or fractional shortening (Supplementary Table S1), similar to what we previously found in a genetic mouse model with systemic FGF23 elevations.[70] When the heparin concentration coinjected with FGF23 was reduced by 2- or 10-fold, changes in echocardiographic parameters were not significant (Figure 5a and b), indicating a dose-dependent effect of heparin on the cardiac actions of FGF23. Second, it has been shown that the induction of kidney injury in wild-type mice

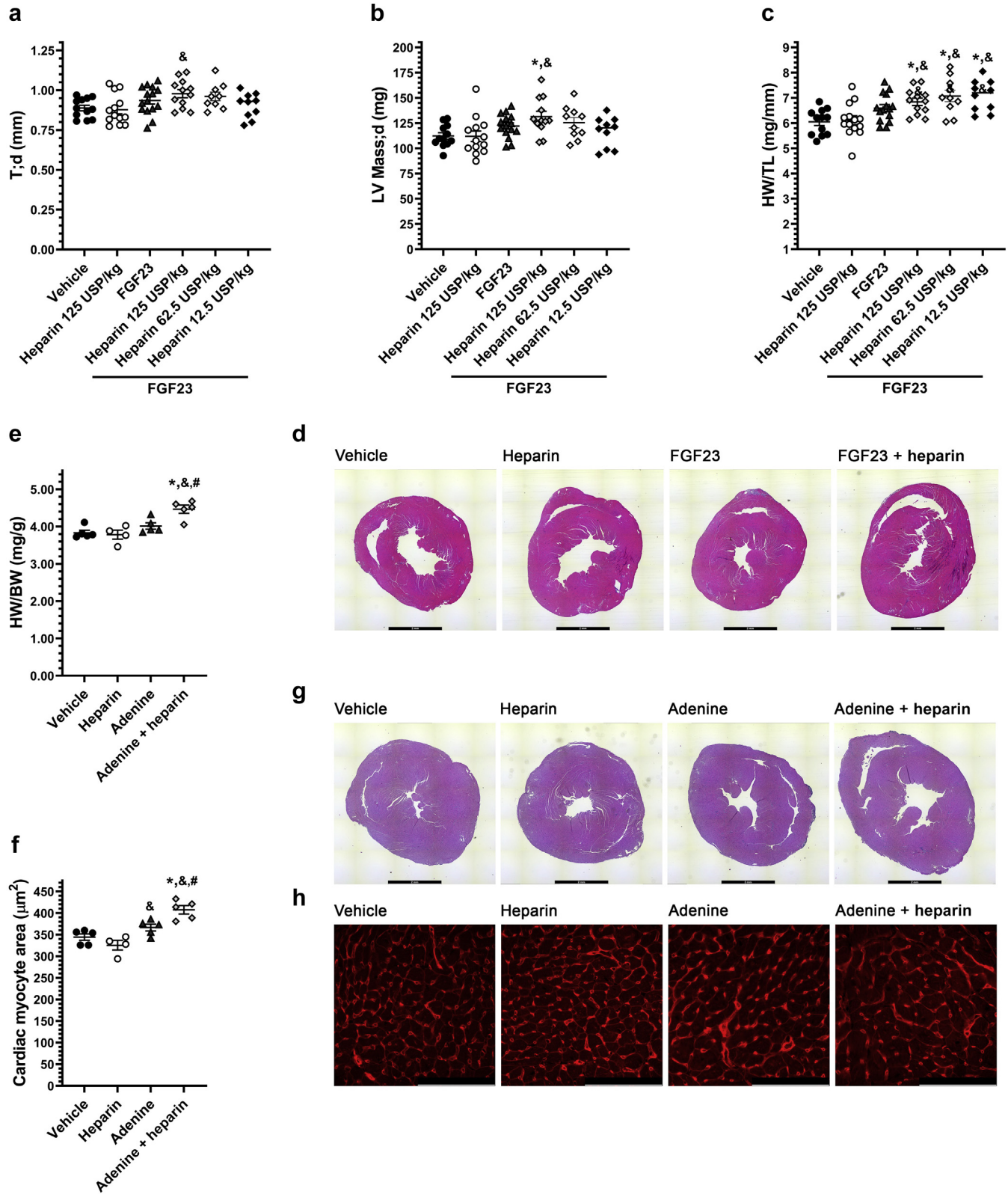

Figure 5 | Frequent heparin injections aggravate cardiac hypertrophy in mouse models with elevated serum fibroblast growth factor (FGF) 23 levels. (**a–d**) Twelve-week-old male BALB/c mice received i.v. injections 2 times per day for 5 consecutive days, with either vehicle (saline), heparin (125 USP/kg), FGF23 (40 μg/kg), or FGF23 (40 μg/kg) plus heparin at 125, 62.5, or 12.5 USP/kg after which mice underwent echocardiographic analysis and were killed. In mice receiving FGF23 and 125 USP/kg of heparin combined, (**a**) average wall thickness of the myocardium (T;d) and (**b**) left ventricular mass in diastole (LV Mass;d) were significantly elevated as compared with vehicle-injected mice. Coinjections of FGF23 with the 2 lower doses of heparin did not result in significant changes. (**c**) Mice receiving FGF23 showed a significant increase in the ratio of heart weight to tibia (continued)

by administration of an adenine-containing diet significantly increases serum FGF23 levels[74] and causes cardiac hypertrophy.[75] Kidney and cardiac injury are more severe in male mice.[76] We placed male and female BALB/c mice on a 0.2% adenine diet for 10 weeks starting at 6 weeks of age. Throughout the feeding study, mice were injected via the tail vein with heparin at 125 USP/kg or saline 3 times per week. After 10 weeks, serum levels of FGF23 and creatinine were significantly elevated in male adenine diet–fed mice when compared with mice on control chow, and heparin injections had no additional effect on these parameters (Supplementary Table S2). These findings indicate that in the adenine diet–fed mouse model, frequent heparin injections do not further elevate circulating FGF23 concentrations or worsen kidney injury. However, compared with mice receiving control chow, adenine mice showed increases in the ratio of heart weight to body weight as well as cross-sectional area of individual myocytes, which both were exacerbated by heparin injections (Figure 5e–h). Heparin injections in mice on a normal diet had no effect on the heart. Furthermore, although female mice on an adenine diet did not develop kidney injury (Supplementary Table S2) or cardiac hypertrophy (Supplementary Figure S4B), they had significantly elevated serum levels of FGF23 and phosphate (Supplementary Table S2). Heparin injections in female adenine mice induced a significant increase in the area of individual cardiac myocytes (Supplementary Figure S4C). Combined, our 2 animal models indicate that although frequent heparin injections by themselves do not affect the heart, they promote cardiac hypertrophy in the presence of systemic FGF23 elevations, as the case in CKD.

DISCUSSION

We found that sKL and heparin act as FGFR coreceptors for FGF23 (Supplementary Figure S5). Both factors bind FGFRs independently from each other and in the absence of FGF23 and thereby increase the FGFR binding affinity for FGF23. sKL mediates FGF23 binding to various FGFR isoforms and favors FGFR1 in the absence of FGF23 and FGFR4 in the presence of FGF23. In contrast, heparin seems to mainly facilitate the FGF23 interaction with FGFR4. Heparin increases FGFR affinities of FGF23 to a lower extent than sKL. Furthermore, we found that sKL and heparin can independently bind FGF23 in the absence of FGFRs and then mediate binding to FGFRs following the same FGFR isoform specificity as detected for the FGFR binding of sKL and heparin that occurs in the absence of FGF23. By doing so, sKL serves as a circulating FGF23 binding partner. However, on the basis of differences in binding affinities, sKL seems to favor the interaction with FGFR1 over FGF23. Our findings also suggest that as known for paracrine FGFs, heparin promotes FGF23 binding to FGFRs in a klotho-independent manner and plays a dual role in the FGFR activation process. Heparin supports the formation of a stable FGF/FGFR/heparin ternary complex as well as FGFR/FGFR dimerization and subsequent activation of signaling events. Although compared to paracrine FGFs the affinity of FGF23 for heparin is lower, heparin can still act as a cofactor for FGF23-FGFR binding and might do so in an FGFR isoform–specific manner. Different from their effects on FGF23, heparin and sKL do not mediate binding of FGF19 or FGF21 to any of the FGFR isoforms, suggesting that not only sKL but also heparin acts as an FGF23-specific FGFR coreceptor.

Our finding that heparin can bind FGF23 is surprising, as it goes against the common conception that as an endocrine FGF, FGF23 underwent changes in the topology of its heparin-binding site during evolution, resulting in a loss of heparin-binding capability.[41] Heparin binding of FGF23 has been previously detected in a nonquantitative manner and with low affinity using heparin columns.[40] Furthermore, heparin columns have been used to purify recombinant FGF23 protein.[65] We provide first quantitative data indicating that the interaction between FGF23 and heparin occurs with high affinity. This is in line with cell-based studies showing that cotreatment with heparin can increase the cellular effects of FGF23.[80,85,88,89] Our finding that sKL can bind heparin is surprising, because klotho does not seem to be in direct contact with heparin within the FGF23/FGFR1/klotho complex.[65] The biological relevance of the sKL-heparin interaction remains to be established. For both sKL and FGF23, the question arises how in the light of high-affinity binding to heparin these proteins can act as endocrine factors.

We propose that our novel mechanistic findings have several important implications for pathologies that are associated with elevated FGF23 levels and reduced klotho expression, such as CKD and associated cardiovascular injury. In the absence of klotho, FGF23 can bind FGFR4 with low affinity and thereby contribute to cardiac hypertrophy. We could confirm the klotho-independent low-affinity binding between recombinant FGF23 and FGFR4 proteins, which was

Figure 5 | (continued) length (HW/TL) when coinjected with each heparin dose as compared with vehicle-injected mice. (**d**) Representative hematoxylin and eosin (H&E) staining of cardiac cross-sections. Bar = 2 mm. (**e–h**) Five-week-old male BALB/c mice were administered a 0.2% adenine diet or control chow. After 1 week, mice were i.v. injected 3 times per week with heparin (125 USP/kg) or saline. (**e**) The ratio of heart weight to body weight (HW/BW) and (**f**) area of individual cardiac myocytes were significantly increased in adenine mice injected with heparin. (**g**) Representative H&E staining of cardiac cross-sections from all groups. Bar = 2 mm. (**h**) Representative images of cardiac wheat germ agglutinin (WGA) staining for the quantification shown in (**g**). Bar = 100 μm. Comparison between groups was performed using 1-way analysis of variance followed by a *post hoc* Tukey test (**a–c,e,f**). A significance level of $P \leq 0.05$ was accepted as statistically significant. (**a–c**) $n = 4–5$. $^{*}P \leq 0.05$ versus vehicle, $^{\&}P \leq 0.05$ versus heparin. (**e,f**) $n = 4–5$. $^{*}P \leq 0.05$ versus vehicle, $^{\&}P \leq 0.05$ versus heparin, $^{\#}P \leq 0.05$ versus adenine. All values are expressed as mean ± SEM. To optimize viewing of this image, please see the online version of this article at www.kidney-international.org.

detectable only by our sensitive plate–based binding assay but not in less sensitive co-immunoprecipitation studies. We found that sKL can bind FGFR4 and thereby increase FGF23 affinity and directly inhibit the pathologic actions of FGF23 on cardiac myocytes. Although the precise mechanism remains unknown, we postulate that sKL might induce a switch from FGF23-induced klotho-independent PLCγ/calcineurin/NFAT to klotho-dependent Ras/MAPK signaling and thereby from FGF23-induced pathologic to protective cardiac events. Alternatively, because sKL has a higher affinity for FGFR1 than for FGFR4, sKL might force FGF23 into FGFR1/sKL binding and signaling and away from klotho-independent prohypertrophic calcineurin/NFAT signaling that is mediated by FGFR4. Our findings set the stage for preclinical CKD studies with the goal to test potential cardioprotective effects of sKL. Administration of sKL could have additional beneficial effects by increasing FGF23 responsiveness in physiologic target organs that, because of injury, have lost klotho expression, such as the kidney in CKD. It is possible that injected sKL binds to remaining FGFR1 molecules on proximal tubular epithelial cells, thereby generating high-affinity FGF23 binding sites, resulting in increased kidney responsiveness to FGF23 and kidney phosphate excretion. Our finding that sKL can block the klotho-independent binding of FGFRs to paracrine FGFs suggests that sKL's beneficial functions are not only based on its modulation of FGF23 signaling but also mediated by the inhibition of mitogenic FGFR1c signaling induced by paracrine FGFs, which potentially results in antifibrotic and/or antitumor effects. We propose that the pleiotropic actions of sKL might be based on its involvement in various FGF-FGFR binding and subsequent signaling events.

Finally, we found that heparin specifically increases FGF23 binding to FGFR4, the FGFR isoform that mediates the pathologic actions of FGF23 on cardiac myocytes,[16,73] and thereby promotes the acute effects of FGF23 on increasing contractility, dysregulating intracellular calcium, and enhancing arrhythmogenicity as well as the prolonged FGF23 effects of inducing hypertrophic cell growth. Combined, these cellular alterations might result in accelerated pathologic cardiac remodeling, as supported by our 2 mouse models with systemic FGF23 elevations, where frequent heparin injections worsened the cardiac phenotype, while heparin injections by themselves in healthy control animals had no cardiac effects. Patients with end-stage renal disease on hemodialysis frequently receive heparin infusions to prevent blood clotting during the dialysis process. Because hemodialysis does not reduce serum FGF23 levels,[90] these patients are exposed to constant systemic elevations of both FGF23 and heparin. Whether heparin injections contribute to the high rates of cardiovascular events and mortality in patients on hemodialysis remains to be studied.

DISCLOSURE

CF has served as a consultant for Bayer and Calico Labs. CY and CF are inventors of 2 pending patents (PCT/US2019/049211 and PCT/US19/49161) aimed to produce and detect bioactive soluble klotho, and they are cofounders of a startup biotech company (Alpha Young LLC) that has the goal to further develop and commercialize these products and assays. CF is currently the CSO of Alpha Young LLC. CF has a patent on fibroblast growth factor receptor inhibition (European Patent No. 2723391). KW received royalties from Kyowa-Hakko-Kirin Pharmaceutics and research funding from Akebia/Keryx and Calico Labs. All the other authors declared no competing interests.

ACKNOWLEDGMENTS

This study was supported by the Deutsche Forschungsgemeinschaft (DK), the National Science Foundation (IC), the American Society of Nephrology (AG), the American Heart Association (GO), and by the National Institutes of Health (grants F31DK115074 [CY], F31DK117550 [BC], P01AG039355 [MJW], P01AG039355-08S2 [MJW and JV], R01HL133011 [ARW], R01HL146111 [MK], R01HL128714 [CF], and R01HL145528 [KW and CF]). RJL was supported by GlycoMIP, a National Science Foundation Materials Innovation Platform funded through Cooperative Agreement DMR-1933525. GR-H was supported by the Instituto de Salud Carlos III cofunded by the European Regional Development Fund (Fondos FEDER, CP15/00129 and PI17/01093) and Fundación Renal Íñigo Álvarez de Toledo (FRIAT). CF was supported by the UAB-UCSD O'Brien Core Center for Acute Kidney Injury Research, the AMC21 program of the Department of Medicine at UAB, and the Tolwani Innovation Award from the Division of Nephrology at UAB.

SUPPLEMENTARY MATERIAL

Supplementary File (PDF)

Figure S1. Soluble klotho (sKL) and heparin do not modify fibroblast growth factor receptor (FGFR) affinities of fibroblast growth factor (FGF) 19 and FGF21.
Figure S2. Soluble klotho (sKL) purification and half-life.
Figure S3. Concept of the soluble klotho (sKL) detection assay.
Figure S4. Frequent heparin injections aggravate cardiac hypertrophy in mouse models with elevated serum fibroblast growth factor (FGF) 23 levels—additional parameters.
Figure S5. Mechanisms for the fibroblast growth factor (FGF) coreceptor activities of soluble klotho (sKL) and heparin.
Table S1. Ultrasound parameters of mice receiving serial fibroblast growth factor (FGF) 23 injections.
Table S2. Serum chemistry of mice receiving an adenine diet.
Table S3. Measurement definitions for B-mode.
Table S4. Calculation definitions for B-mode.
Table S5. Summary of kinetic data of heparin binding to fibroblast growth factor (FGF) 23, FGF receptor isoform 4 (FGFR4), and klotho and of the FGF23-FGFR4 interaction.

REFERENCES

1. Quarles LD. Endocrine functions of bone in mineral metabolism regulation. *J Clin Invest*. 2008;118:3820–3828.
2. Kuro-o M, Matsumura Y, Aizawa H, et al. Mutation of the mouse klotho gene leads to a syndrome resembling ageing. *Nature*. 1997;390:45–51.
3. Urakawa I, Yamazaki Y, Shimada T, et al. Klotho converts canonical FGF receptor into a specific receptor for FGF23. *Nature*. 2006;444:770–774.
4. Saito H, Maeda A, Ohtomo S, et al. Circulating FGF-23 is regulated by 1α, 25-dihydroxyvitamin D3 and phosphorus in vivo. *J Biol Chem*. 2005;280:2543–2549.
5. Shimada T, Hasegawa H, Yamazaki Y, et al. FGF-23 is a potent regulator of vitamin D metabolism and phosphate homeostasis. *J Bone Miner Res*. 2004;19:429–435.
6. Shimada T, Urakawa I, Yamazaki Y, et al. FGF-23 transgenic mice demonstrate hypophosphatemic rickets with reduced expression of

sodium phosphate cotransporter type IIa. *Biochem Biophys Res Commun*. 2004;314:409–414.
7. Saito H, Kusano K, Kinosaki M, et al. Human fibroblast growth factor-23 mutants suppress Na^+-dependent phosphate co-transport activity and 1α,25-dihydroxyvitamin D3 production. *J Biol Chem*. 2003;278:2206–2211.
8. Isakova T, Gutierrez OM, Wolf M. A blueprint for randomized trials targeting phosphorus metabolism in chronic kidney disease. *Kidney Int*. 2009;76:705–716.
9. Isakova T, Wahl P, Vargas GS, et al. Fibroblast growth factor 23 is elevated before parathyroid hormone and phosphate in chronic kidney disease. *Kidney Int*. 2011;79:1370–1378.
10. Isakova T, Xie H, Yang W, et al. Fibroblast growth factor 23 and risks of mortality and end-stage renal disease in patients with chronic kidney disease. *JAMA*. 2011;305:2432–2439.
11. Gutierrez OM, Mannstadt M, Isakova T, et al. Fibroblast growth factor 23 and mortality among patients undergoing hemodialysis. *N Engl J Med*. 2008;359:584–592.
12. Richter B, Faul C. FGF23 actions on target tissues—with and without klotho. *Front Endocrinol (Lausanne)*. 2018;9:189.
13. Faul C, Amaral AP, Oskouei B, et al. FGF23 induces left ventricular hypertrophy. *J Clin Invest*. 2011;121:4393–4408.
14. Touchberry CD, Green TM, Tchikrizov V, et al. FGF23 is a novel regulator of intracellular calcium and cardiac contractility in addition to cardiac hypertrophy. *Am J Physiol Endocrinol Metab*. 2013;304:E863–E873.
15. Singh S, Grabner A, Yanucil C, et al. Fibroblast growth factor 23 directly targets hepatocytes to promote inflammation in chronic kidney disease. *Kidney Int*. 2016;90:985–996.
16. Grabner A, Amaral AP, Schramm K, et al. Activation of cardiac fibroblast growth factor receptor 4 causes left ventricular hypertrophy. *Cell Metab*. 2015;22:1020–1032.
17. Grabner A, Schramm K, Silswal N, et al. FGF23/FGFR4-mediated left ventricular hypertrophy is reversible. *Sci Rep*. 2017;7:1993.
18. Murphy D, McCulloch CE, Lin F, et al. Trends in prevalence of chronic kidney disease in the United States. *Ann Intern Med*. 2016;165:473–481.
19. Tonelli M, Wiebe N, Culleton B, et al. Chronic kidney disease and mortality risk: a systematic review. *J Am Soc Nephrol*. 2006;17:2034–2047.
20. Go AS, Chertow GM, Fan D, et al. Chronic kidney disease and the risks of death, cardiovascular events, and hospitalization. *N Engl J Med*. 2004;351:1296–1305.
21. Zoccali C, Benedetto FA, Mallamaci F, et al. Prognostic value of echocardiographic indicators of left ventricular systolic function in asymptomatic dialysis patients. *J Am Soc Nephrol*. 2004;15:1029–1037.
22. Foley RN, Parfrey PS, Harnett JD, et al. Clinical and echocardiographic disease in patients starting end-stage renal disease therapy. *Kidney Int*. 1995;47:186–192.
23. London GM, Pannier B, Guerin AP, et al. Alterations of left ventricular hypertrophy in and survival of patients receiving hemodialysis: follow-up of an interventional study. *J Am Soc Nephrol*. 2001;12:2759–2767.
24. Paoletti E, Bellino D, Cassottana P, et al. Left ventricular hypertrophy in nondiabetic predialysis CKD. *Am J Kidney Dis*. 2005;46:320–327.
25. Appel LJ, Wright JT Jr, Greene T, et al. Intensive blood-pressure control in hypertensive chronic kidney disease. *N Engl J Med*. 2010;363:918–929.
26. Baigent C, Landray MJ, Reith C, et al. The effects of lowering LDL cholesterol with simvastatin plus ezetimibe in patients with chronic kidney disease (Study of Heart and Renal Protection): a randomised placebo-controlled trial. *Lancet*. 2011;377:2181–2192.
27. Lowrie EG, Huang WH, Lew NL. Death risk predictors among peritoneal dialysis and hemodialysis patients: a preliminary comparison. *Am J Kidney Dis*. 1995;26:220–228.
28. Zager PG, Nikolic J, Brown RH, et al. Medical Directors of Dialysis Clinic, Inc. "U" curve association of blood pressure and mortality in hemodialysis patients. *Kidney Int*. 1998;54:561–569.
29. Gross ML, Ritz E. Hypertrophy and fibrosis in the cardiomyopathy of uremia—beyond coronary heart disease. *Semin Dial*. 2008;21:308–318.
30. Rambausek M, Ritz E, Mall G, et al. Myocardial hypertrophy in rats with renal insufficiency. *Kidney Int*. 1985;28:775–782.
31. Siedlecki AM, Jin X, Muslin AJ. Uremic cardiac hypertrophy is reversed by rapamycin but not by lowering of blood pressure. *Kidney Int*. 2009;75:800–808.
32. Ritz E. Left ventricular hypertrophy in renal disease: beyond preload and afterload. *Kidney Int*. 2009;75:771–773.
33. Ayus JC, Mizani MR, Achinger SG, et al. Effects of short daily versus conventional hemodialysis on left ventricular hypertrophy and inflammatory markers: a prospective, controlled study. *J Am Soc Nephrol*. 2005;16:2778–2788.
34. Winchester JF, Audia PF. Extracorporeal strategies for the removal of middle molecules. *Semin Dial*. 2006;19:110–114.
35. Itoh N, Ornitz DM. Evolution of the *Fgf* and *Fgfr* gene families. *Trends Genet*. 2004;20:563–569.
36. Eswarakumar VP, Lax I, Schlessinger J. Cellular signaling by fibroblast growth factor receptors. *Cytokine Growth Factor Rev*. 2005;16:139–149.
37. Schlessinger J, Plotnikov AN, Ibrahimi OA, et al. Crystal structure of a ternary FGF-FGFR-heparin complex reveals a dual role for heparin in FGFR binding and dimerization. *Mol Cell*. 2000;6:743–750.
38. Ibrahimi OA, Yeh BK, Eliseenkova AV, et al. Analysis of mutations in fibroblast growth factor (FGF) and a pathogenic mutation in FGF receptor (FGFR) provides direct evidence for the symmetric two-end model for FGFR dimerization. *Mol Cell Biol*. 2005;25:671–684.
39. Goetz R, Ohnishi M, Kir S, et al. Conversion of a paracrine fibroblast growth factor into an endocrine fibroblast growth factor. *J Biol Chem*. 2012;287:29134–29146.
40. Asada M, Shinomiya M, Suzuki M, et al. Glycosaminoglycan affinity of the complete fibroblast growth factor family. *Biochim Biophys Acta*. 2009;1790:40–48.
41. Goetz R, Beenken A, Ibrahimi OA, et al. Molecular insights into the klotho-dependent, endocrine mode of action of fibroblast growth factor 19 subfamily members. *Mol Cell Biol*. 2007;27:3417–3428.
42. Harmer NJ, Pellegrini L, Chirgadze D, et al. The crystal structure of fibroblast growth factor (FGF) 19 reveals novel features of the FGF family and offers a structural basis for its unusual receptor affinity. *Biochemistry*. 2004;43:629–640.
43. Kurosu H, Ogawa Y, Miyoshi M, et al. Regulation of fibroblast growth factor-23 signaling by klotho. *J Biol Chem*. 2006;281:6120–6123.
44. Nakatani T, Ohnishi M, Razzaque MS. Inactivation of klotho function induces hyperphosphatemia even in presence of high serum fibroblast growth factor 23 levels in a genetically engineered hypophosphatemic (Hyp) mouse model. *FASEB J*. 2009;23:3702–3711.
45. Chen CD, Podvin S, Gillespie E, et al. Insulin stimulates the cleavage and release of the extracellular domain of klotho by ADAM10 and ADAM17. *Proc Natl Acad Sci U S A*. 2007;104:19796–19801.
46. Chen CD, Tung TY, Liang J, et al. Identification of cleavage sites leading to the shed form of the anti-aging protein klotho. *Biochemistry*. 2014;53:5579–5587.
47. Lindberg K, Amin R, Moe OW, et al. The kidney is the principal organ mediating klotho effects. *J Am Soc Nephrol*. 2014;25:2169–2175.
48. Hu MC, Shi M, Zhang J, et al. Renal production, uptake, and handling of circulating αKlotho. *J Am Soc Nephrol*. 2016;27:79–90.
49. Imura A, Iwano A, Tohyama O, et al. Secreted Klotho protein in sera and CSF: implication for post-translational cleavage in release of Klotho protein from cell membrane. *FEBS Lett*. 2004;565:143–147.
50. Kurosu H, Yamamoto M, Clark JD, et al. Suppression of aging in mice by the hormone Klotho. *Science*. 2005;309:1829–1833.
51. Hu MC, Shiizaki K, Kuro-o M, Moe OW. Fibroblast growth factor 23 and Klotho: physiology and pathophysiology of an endocrine network of mineral metabolism. *Annu Rev Physiol*. 2013;75:503–533.
52. Barker SL, Pastor J, Carranza D, et al. The demonstration of αKlotho deficiency in human chronic kidney disease with a novel synthetic antibody. *Nephrol Dial Transplant*. 2015;30:223–233.
53. Sakan H, Nakatani K, Asai O, et al. Reduced renal α-Klotho expression in CKD patients and its effect on renal phosphate handling and vitamin D metabolism. *PLoS One*. 2014;9:e86301.
54. Hu MC, Shi M, Cho HJ, et al. Klotho and phosphate are modulators of pathologic uremic cardiac remodeling. *J Am Soc Nephrol*. 2015;26:1290–1302.
55. Hu MC, Shi M, Zhang J, et al. Klotho deficiency causes vascular calcification in chronic kidney disease. *J Am Soc Nephrol*. 2011;22:124–136.
56. Yang K, Wang C, Nie L, et al. Klotho protects against indoxyl sulphate-induced myocardial hypertrophy. *J Am Soc Nephrol*. 2015;26:2434–2446.
57. Xie J, Cha SK, An SW, et al. Cardioprotection by Klotho through downregulation of TRPC6 channels in the mouse heart. *Nat Commun*. 2012;3:1238.
58. Xie J, Yoon J, An SW, et al. Soluble klotho protects against uremic cardiomyopathy independently of fibroblast growth factor 23 and phosphate. *J Am Soc Nephrol*. 2015;26:1150–1160.
59. Grabner A, Faul C. The role of fibroblast growth factor 23 and Klotho in uremic cardiomyopathy. *Curr Opin Nephrol Hypertens*. 2016;25:314–324.

60. Hu MC, Shi M, Zhang J, et al. Klotho: a novel phosphaturic substance acting as an autocrine enzyme in the renal proximal tubule. *FASEB J*. 2010;24:3438–3450.
61. Chang Q, Hoefs S, van der Kemp AW, et al. The β-glucuronidase klotho hydrolyzes and activates the TRPV5 channel. *Science*. 2005;310:490–493.
62. Cha SK, Ortega B, Kurosu H, et al. Removal of sialic acid involving Klotho causes cell-surface retention of TRPV5 channel via binding to galectin-1. *Proc Natl Acad Sci U S A*. 2008;105:9805–9810.
63. Dalton G, An SW, Al-Juboori SI, et al. Soluble klotho binds monosialoganglioside to regulate membrane microdomains and growth factor signaling. *Proc Natl Acad Sci U S A*. 2017;114:752–757.
64. Dalton GD, Xie J, An SW, Huang CL. New insights into the mechanism of action of soluble klotho. *Front Endocrinol (Lausanne)*. 2017;8:323.
65. Chen G, Liu Y, Goetz R, et al. α-Klotho is a non-enzymatic molecular scaffold for FGF23 hormone signalling. *Nature*. 2018;553:461–466.
66. Ogawa Y, Kurosu H, Yamamoto M, et al. βKlotho is required for metabolic activity of fibroblast growth factor 21. *Proc Natl Acad Sci U S A*. 2007;104:7432–7437.
67. Shi SY, Lu YW, Liu Z, et al. A biparatopic agonistic antibody that mimics fibroblast growth factor 21 ligand activity. *J Biol Chem*. 2018;293:5909–5919.
68. Shalhoub V, Shatzen EM, Ward SC, et al. FGF23 neutralization improves chronic kidney disease-associated hyperparathyroidism yet increases mortality. *J Clin Invest*. 2012;122:2543–2553.
69. Navarro-García JA, Delgado C, Fernandez-Velasco M, et al. Fibroblast growth factor-23 promotes rhythm alterations and contractile dysfunction in adult ventricular cardiomyocytes. *Nephrol Dial Transplant*. 2019;34:1864–1875.
70. Wacker MJ, Touchberry CD, Silswal N, et al. Skeletal muscle, but not cardiovascular function, is altered in a mouse model of autosomal recessive hypophosphatemic rickets. *Front Physiol*. 2016;7:173.
71. Avin KG, Vallejo JA, Chen NX, et al. Fibroblast growth factor 23 does not directly influence skeletal muscle cell proliferation and differentiation or ex vivo muscle contractility. *Am J Physiol Endocrinol Metab*. 2018;315:E594–E604.
72. Andrukhova O, Slavic S, Smorodchenko A, et al. FGF23 regulates renal sodium handling and blood pressure. *EMBO Mol Med*. 2014;6:744–759.
73. Han X, Cai C, Xiao Z, Quarles LD. FGF23 induced left ventricular hypertrophy mediated by FGFR4 signaling in the myocardium is attenuated by soluble Klotho in mice. *J Mol Cell Cardiol*. 2019;138:66–74.
74. Jia T, Olauson H, Lindberg K, et al. A novel model of adenine-induced tubulointerstitial nephropathy in mice. *BMC Nephrol*. 2013;14:116.
75. Clinkenbeard EL, Noonan ML, Thomas JC, et al. Increased FGF23 protects against detrimental cardio-renal consequences during elevated blood phosphate in CKD. *JCI Insight*. 2019;4:e123817.
76. Diwan V, Small D, Kauter K, et al. Gender differences in adenine-induced chronic kidney disease and cardiovascular complications in rats. *Am J Physiol Renal Physiol*. 2014;307:F1169–F1178.
77. Goetz R, Ohnishi M, Ding X, et al. Klotho coreceptors inhibit signaling by paracrine fibroblast growth factor 8 subfamily ligands. *Mol Cell Biol*. 2012;32:1944–1954.
78. Hu MC, Shi M, Gillings N, et al. Recombinant α-Klotho may be prophylactic and therapeutic for acute to chronic kidney disease progression and uremic cardiomyopathy. *Kidney Int*. 2017;91:1104–1114.
79. Navarro-Garcia JA, Salguero-Bodes R, Gonzalez-Lafuente L, et al. The anti-aging factor Klotho protects against acquired long QT syndrome induced by uremia and promoted by fibroblast growth factor 23. *BMC Med*. 2022;20:14.
80. Xiao Z, King G, Mancarella S, et al. FGF23 expression is stimulated in transgenic α-Klotho longevity mouse model. *JCI Insight*. 2019;4:e132820.
81. Wang Q, Su W, Shen Z, Wang R. Correlation between soluble α-Klotho and renal function in patients with chronic kidney disease: a review and meta-analysis. *Biomed Res Int*. 2018;2018:9481475.
82. Olauson H, Mencke R, Hillebrands JL, Larsson TE. Tissue expression and source of circulating αKlotho. *Bone*. 2017;100:19–35.
83. Gao G, Goldfarb M. Heparin can activate a receptor tyrosine kinase. *EMBO J*. 1995;14:2183–2190.
84. Loo BM, Kreuger J, Jalkanen M, et al. Binding of heparin/heparan sulfate to fibroblast growth factor receptor 4. *J Biol Chem*. 2001;276:16868–16876.
85. Yu X, Ibrahimi OA, Goetz R, et al. Analysis of the biochemical mechanisms for the endocrine actions of fibroblast growth factor-23. *Endocrinology*. 2005;146:4647–4656.
86. Slavic S, Ford K, Modert M, et al. Genetic ablation of Fgf23 or klotho does not modulate experimental heart hypertrophy induced by pressure overload. *Sci Rep*. 2017;7:11298.
87. Han X, Ross J, Kolumam G, et al. Cardiovascular effects of renal distal tubule deletion of the FGF receptor 1 gene. *J Am Soc Nephrol*. 2018;29:69–80.
88. Zhang X, Ibrahimi OA, Olsen SK, et al. Receptor specificity of the fibroblast growth factor family: the complete mammalian FGF family. *J Biol Chem*. 2006;281:15694–15700.
89. Shalhoub V, Ward SC, Sun B, et al. Fibroblast growth factor 23 (FGF23) and α-klotho stimulate osteoblastic MC3T3.E1 cell proliferation and inhibit mineralization. *Calcif Tissue Int*. 2011;89:140–150.
90. Wolf M. Forging forward with 10 burning questions on FGF23 in kidney disease. *J Am Soc Nephrol*. 2010;21:1427–1435.